Annual Progress Report

for

"Laboratory Simulation of Field-Aligned Currents"

NASA Contract Award No. NAGW - 2655

Progress Reporting Period 3 /92-3/93

Principal Investigators:

Frank J. Wessel

Norman Rostoker

Department of Physics

University of California

Irvine, CA 92717

Research Objectives

- To simulate, via laboratory experiments, the three terms of the field-aligned current equation (Hasegawa and Sato, Dynamics of the Magnetosphere, by S. I. Akasofu, p. 529, D. Reidel Pub. Co., Dordrecht, Holland, 1979),

$$J_{\parallel} = B \int_0^{l_{\parallel}} \left[\frac{\rho}{B} \frac{d}{dt}\left(\frac{\Omega}{B}\right) + \frac{2}{B^2} J_{\perp} \cdot \nabla B + \frac{1}{\rho B} J_{in} \cdot \nabla \rho \right] dl_{\parallel}$$

- To simulate auroral-arc formation processes by configuring the boundary conditions of the experimental chamber and plasma parameters to produce highly localized return currents at the end of a field-aligned current system.

- To extrapolate these results, using theoretical and computational techniques, to the problem of magnetospheric-ionospheric coupling and to compare them with published-literature signatures of auroral-arc phenomena.

PROGRESS PERIOD: April92-March 93

A summary of our progress is contained in the following attachments:

1. Abstract and poster pages for "Laboratory simulation of magnetospheric field aligned currents," presented at the fall 1992 meeting of the AGU,

2. University of California, internal report on "Characterization of a deflagration plasma gun," used as the basis of the dynamo plasma in the medium energy plasma beam facility ($V_0 \simeq 15$ cm/μsec = 140 km/sec, $n_0 \leq 10^{14}$ cm^{-3}); the high energy beam facility was described in the 1991 annual report,

3. Journal arcticle on "Propagation of a narrow plasma beam in an oblique magnetic field" published in Phys. Fluids October 1992,

4. Journal arcticle on the "Dynamic behavior of the magnetotail in a laboratory magnetosphere" submitted to Journal of Geophysics,

Attachment 1.

Abstract and poster pages for
"Laboratory simulation of magnetospheric field aligned currents,"
presented at the 1992 fall meeting of the American Geophysical Union

astrophysical plasmas. The instability at the magnetospheric boundary is a prototype of a number of similar problems in space physics and astrophysics such as the heliopause stability, the ionopause stability, and the viscosity in the accretion disks. In order to understand the consequences of this instability at the magnetospheric boundary the dependence of the development of the K-H instability on the magnetosheath sonic Mach number M_S is studied in detail by means of a two-dimensional MHD simulation. It is found that a finite thick velocity shear layer with super-Alfvénic velocity jump at the low-latitude magnetospheric boundary is unstable to the K-H instability no matter how large the magnetosheath sonic Mach number; a result suggesting that the tail flank boundary of the magnetosphere is also unstable to the K-H instability. For all magnetosheath sonic Mach numbers a velocity boundary layer is formed by the instability inside of the magnetopause. A flow vortex is excited at the inner edge of the velocity boundary layer for all sonic Mach numbers, and the magnetopause boundary is more highly nonlinearly corrugated by the instability for a smaller sonic Mach number. The momentum flux density into the magnetosphere by the instability or the tangential (shearing) stress at the boundary is mostly caused by the Reynolds stress $-\langle \rho v_x v_y \rangle$ associated with the instability and approximated for $1.0 < M_S < 3.0$ by αp_0, where p_0 is the unperturbed magnetosheath pressure and $\alpha = 0.083$. The calculation of the convection potential drop across the velocity boundary layer due to the K-H induced tangential stress gives a reasonable magnitude of the residual convection potential drop. Finally the line-tying effect on the K-H instability is briefly discussed by using a three-dimensional MHD linear analysis. Although the line-tying has a stabilizing influence on the K-H unstable modes, the growth rate does not become zero for $\Sigma_P \to \infty$ when the K-H unstable mode is allowed to have nodes at the ionospheric boundaries.

SM31A-11 0815h POSTER

Ionospheric Signatures of Electromagnetic Ion Cyclotron Waves Recorded by DE-2 Near the Plasmapause

R E Erlandson (The Johns Hopkins University Applied Physics Laboratory, Laurel, MD 20723)
T L Aggson, J A Slavin (Both at: NASA/GSFC Code 696, Greenbelt, MD 20771)

Large amplitude electromagnetic ion cyclotron waves with frequencies on the order of 1 Hz were observed by the magnetometer and vector electric field instruments on the DE-2 satellite in the ionosphere. EMIC waves have been found to propagate parallel to B from their source region in the equatorial magnetosphere to the ionosphere and eventually the ground. In the equatorial magnetosphere, EMIC waves are often observed continuously for many hours and have amplitudes on the order of 1 nT. In contrast, EMIC waves recorded in the ionosphere using DE-2 are observed for time periods on the order of 10 s and have amplitudes which reach 60 nT (45 mV/m in the electric field). Observations from four different events are used to discuss the relationship between EMIC wave signatures in the equatorial magnetosphere and ionosphere.

SM31A-12 0815h POSTER

Is There a Hidden Order in Boundary Layer Data?

M A Hapgood and D A Bryant (Rutherford Appleton Laboratory, Chilton, Didcot, Oxfordshire, OX11 0QX, UK)

We describe a technique which reveals unexpected order in boundary layer data. Electron data (N_e and $T_\perp$) are used to generate a *transition parameter* $\mathcal{T}$, which measures the state of the plasma in the transition between the magnetosheath (high N_e, low $T_\perp$, $\mathcal{T} = 0$) and the magnetosphere (low N_e, high $T_\perp$, $\mathcal{T} = 100$). When plotted against $\mathcal{T}$ many independent plasma measurements form clear patterns. These patterns suggest that $\mathcal{T}$ is, in some as yet unknown way, related to the structure of boundary layer and so can be used to reveal order which is hidden in the time series plots normally used in space physics. The derivation of $\mathcal{T}$ is presented in detail and its application to both macroscopic (e.g. magnetic field strength and direction, ion flow speed and direction) and microscopic data (e.g. electron spectra and anisotropy) is discussed. Some possible relationships between $\mathcal{T}$ and the boundary layer structure are discussed.

SM31A-13 0815h POSTER

Laboratory Simulation of Magnetospheric Field-aligned Currents*

S Drum F J Wessel W W Heidbrink J Manson (University of California, Irvine, CA 92717; 714-856-6854)
G Rostoker (Institute of Earth and Planetary Physics, University of Alberta, Edmonton, Alberta, Canada 403-492-1061)

Field-aligned currents which cause the aurorae are thought to be generated in the magnetosphere. In the MHD-derived theory of Hasegawa and Sato these currents are driven by the time-derivative of the solar wind's vorticity as it interacts with the magnetopause.

Direct satellite observations are incomplete, and simulations of the entire magnetosphere fail to scale all the parameters properly. Therefore we are simulating only a small region of velocity shear, in which vorticity-driven currents should be identifiable by their strong, characteristic dependence on boundary conditions.

Using single- and double-sided Faraday cups to measure flows in a fast ion beam interacting with a dense background plasma in a magnetic field, we have observed asymmetries in the plasma flows that are strongly suggestive of such currents.

Attempts to measure the currents with Rogowski coils are underway; these probes measure currently directly and are less invasive, but have a poor signal-to-noise ratio.

In addition, a deflagration gun producing 50 A/sq. cm. has been built in order to study other parameter regimes.

* Work supported by NASA

SM31A-14 0815h POSTER

The Kelvin-Helmholtz Instability in the Low-Latitude Boundary Layer

J U Brackbill (Los Alamos National Laboratory, Los Alamos NM 87545; ph. 505-667-8811; fax. 505-665-5926; Internet jub@celeste.lanl.gov)

Recent work of Miura explores the dependence of the Kelvin-Helmholtz (KH) instability on the Mach number, M, in a sequence of initial value calculations for $1 < M < 4$ [1]. In Miura's results, the instability persists at high M, but the large eddies one sees with the KH instability at low M are replaced by multiple shocks at high M. We extend Miura's work by considering accelerated flow where M varies spatially from subsonic to supersonic. Using FLIP-MHD [2] and a new adaptive grid generator [3] to model curvilinear geometry, we consider the evolution of an unstable shear layer in a curved boundary layer similar to the flow geometry in the low-latitude boundary layer. The boundary conditions describe a curved expansion fan, with prescribed subsonic inflow conditions on one boundary, and supersonic outflow on another. The flow accelerates through a sonic point as it pass from inflow to outflow. In the results, large eddies formed by the KH instability in the subsonic flow upstream are convected into the supersoni

[1] Akira Miura, J. Geophys. Rsch. 97, 10655 (1992). [2] J U Brackbill, J. Comput. Phys. 96, 163 (1991). [3] J U Brackbill, An adaptive grid generator with directional control, J. Comput. Phys. (1992-submitted).

SM31A-15 0815h POSTER

Observations and Particle Simulations of the Plasma Sheet Boundary Layer Under Stressed Conditions

G Ganguli and H Romero (Space Plasma Branch, Plasma Physics Division, Naval Research Laboratory, Washington DC 20375)

P B Dusenbery (Astrophysical, Planetary, and Atmospheric Sciences, University of Colorado, Boulder, CO 80309)

ISEE field and particle data is presented of several crossings of the Plasma Sheet Boundary Layer (PSBL) covering both active and quite times. The goal of the observational study is to chracterise the nature of the PSBL-Lobe interface. Under stressed conditions, the width of the layer over which the plasma density increases can be of the order of the local ion Larmor radius (several hundred kilometers). A theory is presented of the various linear instabilities that can be given rise to by the highly nonuniform nature of this structure. The nonlinear relaxation mechanisms operative in the PSBL are examined using a particle in cell (PIC) code. Intense lower hybrid turbulence is excited which causes significant perpendicular ion acceleration and the development of a broadbanded power spectrum, extending from below the lower hybrid frequency to the electron plasma frequency.

Work supported by ONR.

SM31B CA: 103 Wed 0830h
Van Allen Lecture: Magnetospheric Convection *(joint with SA,SH)*
Presiding: A Nagy, Univ of Michigan

SM31B-1 0830h INVITED

CONVECTION IN THE EARTH'S MAGNETOSPHERE

Charles F. Kennel (Department of Physics, University of California at Los Angeles, CA 90024-1547)

Axford and Hines proposed in 1961 that a collisionless interaction that mimics viscosity at the magnetopause leads to a circulation of the plasma within the magnetospheric cavity. Plasma is dragged by the solar wind from the dayside to the nightside along what are today called the low-latitude boundary layers, and returns back to the dayside in the interior of the magnetosphere. So, plasma and energy first approaches the earth not from the direction of the sun but from the night-side, illuminating why the aurora is most intense and active at night even though the sun is the ultimate source of the energy for geomagnetic activity. The convection model linked auroral activity to magnetospheric convection, convection to the solar wind, which in its turn extended back to the sun. The once utterly mysterious relationships between geomagnetic, auroral, and solar activity were one step further along the way to being understood.

In 1961, Dungey set forth his own model of convection, driven by resistive reconnection of the interplanetary and geomagnetic fields at the dayside magnetopause. In this circumstance, solar wind plasma and energy enters the magnetosphere flowing anti-sunward over the geomagnetic poles in what are today called the polar cusps or mantles. In either model, the convecting plasma should return to the dayside in the plasma sheet. Despite this basic similarity, the two models could be easily distinguished. In Dungey's model convection is strongest when the interplanetary magnetic field is southward. Open field lines will connect the earth's magnetic polar caps directly to the interplanetary magnetic field. There is a very low-density magnetic tail, a current layer and a sheet of hot plasma separating its two lobes, a magnetic neutral line terminates that plasma sheet, and tailward flow on open field lines is downstream of that neutral line.

It was apparent at once that Dungey's steady reconnection model could not be realistic. It is difficult to find periods of calm solar wind field, so magnetospheric convection should be rarely if ever steady. The observations of magnetopause motions, of ionospheric flows, transient micropulsations, transient auroras and F-region density patches in the high-latitude ionosphere are all tied together by the notion that bursty magnetopause reconnection organizes an unsteady convective flow with a 10-20 minute characteristic time scale. The plasma sheet responds bumpily to the complex input coming to it from the dayside. The flow is rarely even in carefully chosen time intervals in which the interplanetary and geomagnetic variability is small. A historical survey of bursty flows and particle acceleration in the plasma sheet suggests that fast convection is highly intermittent. Under way spacecraft in the plasma sheet encounters bursts of fast flow as those envisioned in the reconnection model at best 10 percent of the time; otherwise, it is immersed in a slow chaotic flow. From this one is tempted to connect with Axford and Hines' original idea about collisionless viscosity. *Work supported by NSF

SM31C CA: 103 Wed 09.
Nonlinear Particle Dynamics
Presiding: T Speiser, Univ of Colorado Boulder

SM31C-1 0945h

Particle Orbits in a Dynamic Magnetotail

J. Birn (Los Alamos National Laboratory, SST-8, MS D4 Alamos, New Mexico 87545)
M. Hesse (NASA/Goddard Space Flight Center, Greenbe 20771)

We investigate ion orbits in the selfconsistent electric and magnetic fields obtained from a resistive MHD simulation of magnetotail dynamics. The MHD simulation, representing plasmoid formation and ejection through a near-Earth reconnection process, gives cross-tail electric fields of up to about 4 mV/m, which lead to integrated potential differences across the tail of up to 200 kV. Ion acceleration is found to occur over a wide range along the tail as a consequence of the enhanced electric field associated with the tailward moving plasmoid and its limited extent in the y direction. We also discuss the spatial extent and the source regions of accelerated particles in the near tail. These particles occupy a significant portion of the closed field line region inside of the separatrix at moderate energies of tens of keV; however, this region is not adjacent to the separatrix.

SM31C-2 1000h

General Consequences of Time Dependence for Single Particle Dynamics in a Magnetic Reversal.

S C Chapman(Space and Plasma Physics Group, School of Mathematical Physical Sciences, University of Sussex, Falmer, Brighton, E. Sussex 9QH, England; ph. 44-273-678455, 44-273-678097;Internet:sandrac@syma.sussex.ac.uk)

We investigate single charged particle dynamics in the earth's prereversal geotail by means of a simple model for the magnetic reversal. The general time dependence, and includes a corresponding inductive electric field. The time dependent Hamiltonian of particle motion in this model describes a system of two coupled oscillators with time dependent frequencies. Particle motion is regular if the frequencies remain seperated; the motion is either a fast Larmor oscillation about the field with a slow bounce between mirror points, or a fast oscillation with slow reversal with a slow orbit about the linking field. If the frequencies approach each other then the motion may become chaotic.

Here we will use the scale free property of the model to investigate control parameters which at any time characterize the particle motion. The 'transition parameter', essentially determined by the particle gyrofrequency ratio, gives the time when the explicit time dependence of the model produces a transition from one regime of behaviour to another. The 'system adiabaticity parameter' indicates whether the pseudoperiod with which the particle moves is changing on a timescale which is fast or slow w.r.t. the particle oscillation period. This will determine the nature of the particle behaviour in any given regime.

For an increasingly thinning reversal of general time dependence we show that both regular Larmor trajectories and chaotic trajectories can persist for a finite time period. A specific model is given which allows determination of these times. If the onset of chaotic behaviour is important in the substorm onset process this approach will provide conditions required for substorm onset.

LABORATORY SIMULATION OF FIELD ALIGNED CURRENTS

S. Drum, F. J. Wessel, W. W. Heidbrink, J. Manson
University of California, Irvine, CA

and

G. Rostoker, Institute of Earth and Planetary Physics
University of Alberta, Edmonton, Alberta, Canada

and

H. U. Rahman and G. Yur
Institute of Geophysics and Planetary Physics
University of California, Riverside, CA

Laboratory Simulation of Magnetospheric Field-aligned Currents*

S Drum F J Wessel W W Heidbrink J Manson (University of California, Irvine, CA 92717; 714-856-6854)
G Rostoker (Institute of Earth and Planetary Physics, University of Alberta, Edmonton, Alberta, Canada 403-492-1061)

Field-aligned currents which cause the aurorae are thought to be generated in the magnetosphere. In the MHD-derived theory of Hasegawa and Sato these currents are driven by the time-derivative of the solar wind's vorticity as it interacts with the magnetopause.

Direct satellite observations are incomplete, and simulations of the entire magnetosphere fail to scale all the parameters properly. Therefore we are simulating only a small region of velocity shear, in which vorticity-driven currents should be identifiable by their strong, characteristic dependence on boundary conditions.

Using single- and double-sided Faraday cups to measure flows in a fast ion beam interacting with a dense background plasma in a magnetic field, we have observed asymmetries in the plasma flows that are strongly suggestive of such currents.

Attempts to measure the currents with Rogowski coils are underway; these probes measure currently directly and are less invasive, but have a poor signal-to-noise ratio.

In addition, a deflagration gun producing 50 A/sq. cm. has been built in order to study other parameter regimes.

* Work supported by NASA

INTRODUCTION

- WE ARE ATTEMPTING TO SIMULATE "MICROSCALE PROCESSES" WHICH CONTRIBUTE TO THE GENERATION OF FIELD-ALIGNED CURRENTS

- THE TECHNIQUE INVOLVES THE FLOW OF A "FAST" PLASMA BEAM WITH A TRANSVERSELY MAGNETIZED "LOW ENERGY" PLASMA

- SCALING CONSIDERATIONS DEMAND THE USE OF THREE TYPES OF PLASMA SOURCES IN ORDER TO REPRODUCE THE RANGE OF PHENOMENA CHARACTERISTIC OF THE MAGNETOSPHERE → IONOSPHERE.

SOURCE TERMS FOR FACs

$$\nabla \cdot J_{\parallel} = - \nabla \cdot J_{\perp}$$

$$\bar{J}_{\perp} = \bar{J}_D + \bar{J}_{IN}$$

$$\bar{J}_D = \bar{B} \times \nabla p / B^2$$

$$\bar{J}_{IN} = -\rho / B^2 \frac{d\bar{V}}{dt} \times \bar{B}$$

MAGNETOSPHERE:

$$\bar{J}_{\parallel} = B \int_0^{l_{\parallel}} \left[\rho / B \frac{d}{dt}\left(\frac{\Omega}{B}\right) + \frac{2}{B^2} \bar{J}_{\perp} \cdot \bar{\nabla} B + \frac{1}{\rho B} J_{IN} \cdot \nabla \rho \right] dl_{\parallel}$$

$$\Omega = (\nabla \times V) \cdot \bar{B} / B$$

IONOSPHERE

$$J_{\parallel} \sin\chi = \Sigma_P \bar{\nabla} \cdot \bar{E}_{\perp} + \frac{\Sigma_H}{B} \bar{\nabla} \cdot (\bar{B} \times \bar{E}_{\perp}) + \frac{\bar{B} \times \bar{E}_{\perp}}{B} \cdot \nabla \bar{\Sigma}_H$$

$$J_{\perp} = \Sigma_{\perp} \bar{E}_{\perp} + \Sigma_{\perp\perp} (\bar{B} \times \bar{E}_{\perp}) / B$$

EXPERIMENTAL CONFIGURATION TO SIMULATE FIELD-ALIGNED CURRENTS

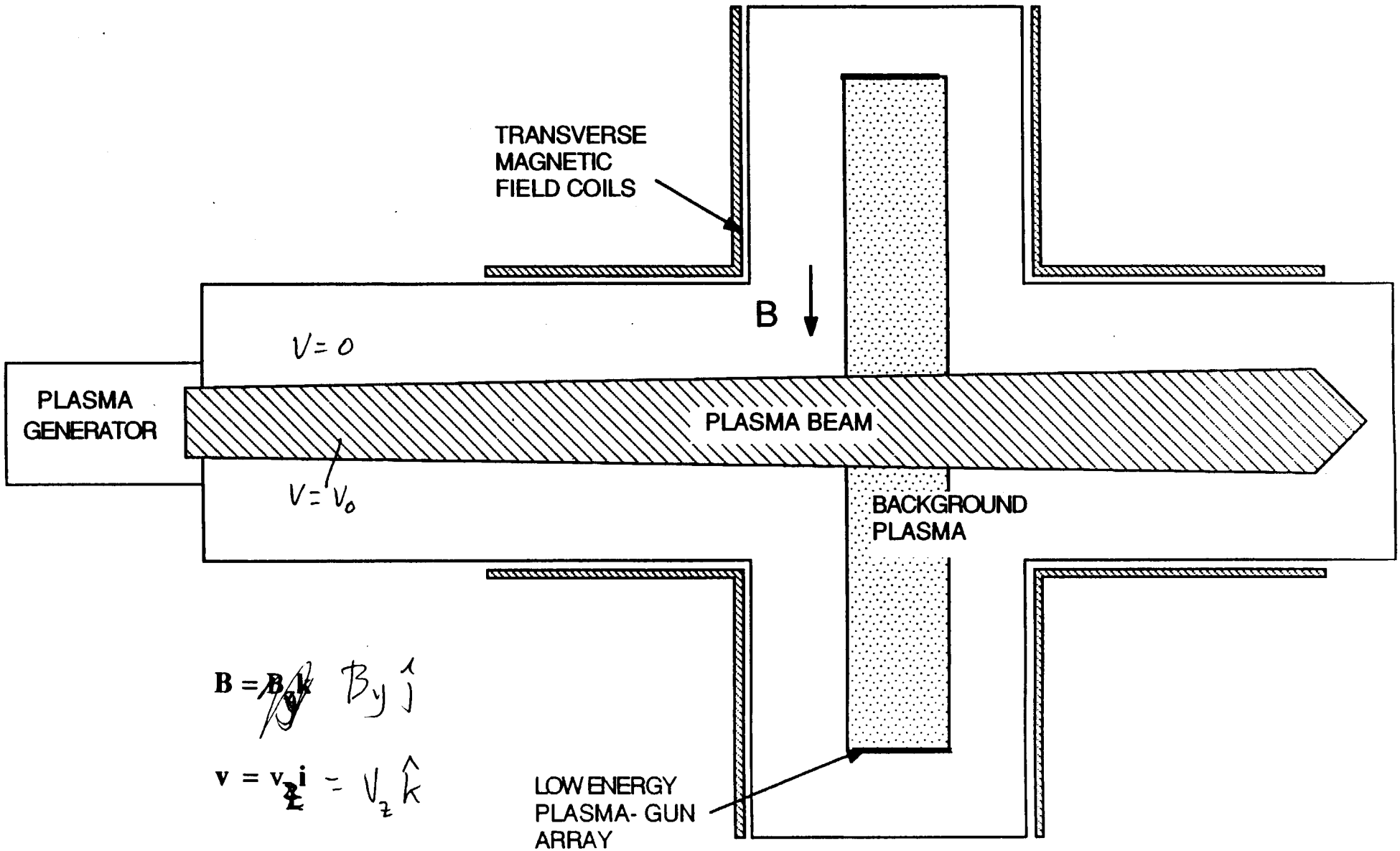

SCALING

The limitations of the MHD approximation[3] can be appreciated by considering the **generalized** Ohm's law,[4]

$$\mathbf{E}^* = \mathbf{J}/\sigma + (1/nec)\,\mathbf{J} \times \mathbf{B} - 1/n\,\nabla\cdot\mathbf{P} + (m_e/ne^2)\partial\mathbf{J}/\partial t \ .$$

where $\mathbf{E}^*$ is the electric field in the co-moving frame of reference,

$$\mathbf{E}^* = \mathbf{E} + \mathbf{V} \times \mathbf{B}/c$$

It is usually assumed that the plasma and magnetic field interact strongly so that terms associated with $\mathbf{E}^*$ are neglected and

$$\mathbf{E} = -\mathbf{V} \times \mathbf{B}/c$$

Which is generally not valid throughout the magnetosphere.

---

[3] Siscoe, G. L., Solar System Magnetohydrodynamics, in Solar-Terrestrial Physics, R. L. Carovillano and J M. Forbes, Editors, D. Reidel Publishing Co., Dordrecht-Holland, 1983, p. 11.

[4] Spitzer, L., Physics of Fully Ionized Gases, Wiley, New York, 1962, p. 28.

SCALING (contd)

Comparison of the magnitude of individual terms in **E*** relative to **V** x **B** (the frozen-in-field term) reveals the dominant forces acting on the flowing magnetoplasma, characterized by the coefficients:

$$R_M^{-1} = \text{(collisional/frozen-in-field)} = (c/\omega_{pe})^2 (X_o V_o \tau_{ei})^{-1}$$
$$R_H^{-1} = \text{(Hall/frozen-in-field)} = M_A^{-2} \rho_i / X_o$$
$$R_P^{-1} = \text{(pressure/frozen-in-field)} = (M_s/M_A)^2 \rho_i / X_o$$
$$R_I^{-1} = \text{(inertial/frozen-in-field)} = (c/\omega_{pe})^2 (X_o V_o t_o)^{-1}$$

The condition $R_M >> 1$ leads to a further condition for MHD behavior, using the momentum equation and neglecting the pressure-gradient term, $\rho d\mathbf{V}/dt \cong \mathbf{J} \times \mathbf{B}/c$, that

$$L = \frac{\sigma}{c^2} B X_o \sqrt{4\pi/\rho} >> 1$$

where L is the Lundquist number, and ρ is the mass density.

Table 1. Approximate plasma parameters and dimensionless scaling parameters for laboratory simulation experiments and the magnetospheric/ionospheric space plasma.

	LABORATORY PLASMA SOURCES			MAGNETOSPHERE			
Parameter	High Energy Sources	Medium Energy Sources	Low Energy Sources	Magnetopause[1]	Low-Lat. Bound. Layer[2]	Central Plasma Sheet[3]	Ionosphere[4]
B(G)	10^2-10^3	10^2-10^3	$< 10^4$	5×10^{-5}	2×10^{-4}	10^{-4}	0.5
n(cm^{-3})	$< 2.5\times10^{11}$	$< 10^{13}$	$< 10^{14}$	5	5	0.5	10^4
T(eV)	200	5	1	1	200	10^3	0.1
V_o(cm/s)	3×10^8	5×10^6	2.5×10^6	3.5×10^7	10^7	5×10^6	10^5
X_o(cm)	50	50	10	6×10^8	10^8	3×10^9	10^7
R_M^{-1}	2×10^{-7}	3×10^{-3}	0.3	10^{-10}	10^{-12}	10^{-14}	0.7
R_H^{-1}	0.1-1	0.2-2	2	3×10^{-3}	0.1	0.06	4
R_p^{-1}	$0.3\text{-}3\times10^{-2}$	$0.5\text{-}5\times10^{-2}$	8×10^{-4}	10^{-4}	0.1	0.1	7×10^{-7}
R_I^{-1}	5×10^{-4}	10^{-5}	3×10^{-5}	10^{-7}	5×10^{-6}	6×10^{-8}	3×10^{-7}
L	$0.3\text{-}3\times10^7$	$0.2\text{-}2\times10^4$	10^3	10^9	2×10^{12}	10^{15}	10^8
ρ_i/X_o	0.6-6	0.01-0.1	10^{-3}	0.1	0.05	10^{-3}	10^{-4}
M_A	0.7-7	0.07-0.7	10^{-2}	7	0.5	0.16	4×10^{-3}
M_S	16	2	2	30	0.56	10^{-1}	1

---

1. Approx. 12 R_E near equitorial latitudes. 2. Approx. 15 R_E near equitorial latitudes. 3. Approx. 30 R_E near equitorial latitudes. 4. Approx. 150 km near 75° latitude, surrounding the polar cap.

$R_M^{-1} = c^2/4\pi\sigma X_o V_o$; $R_H^{-1} = M_A^{-2}(\rho_i/X_o)$; $R_p^{-1} = (M_A/M_S)^2(\rho_i/X_o)$; $R_I^{-1} = (c/\omega_{pe})^2(X_o V_o t_o)^{-1}$

$M_A = V_o/V_{Alfven}$; $M_S = V_o/C_{sound}$; $L = (c/\omega_{pe})^{-2} B X_o \tau_{ei}(nm)^{-1/2}$; $\tau_{ei} = 2.91\times10^{-5}\, n/T^{-3/2}$.

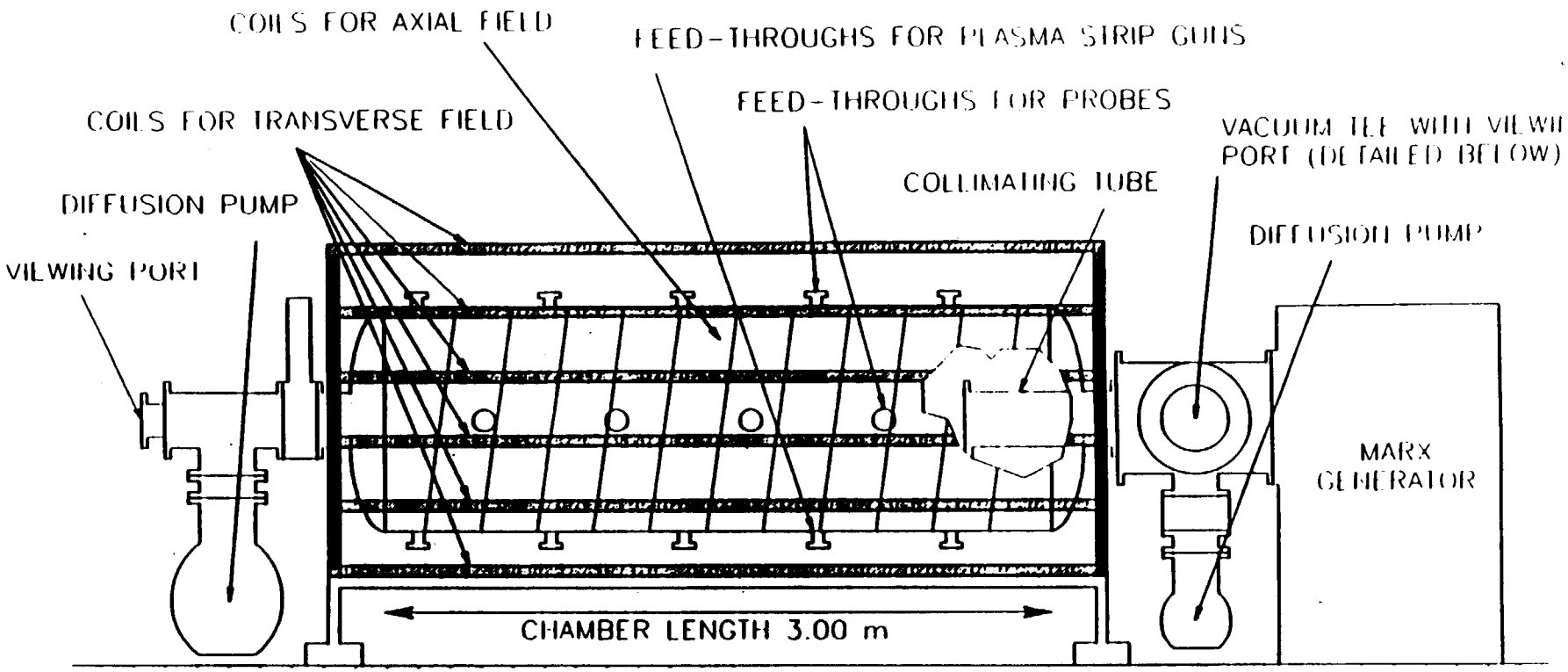

A

Y
Z

DETAIL OF INTERIOR OF CHAMBER SHOWING PLASMA BEAM SOURCE

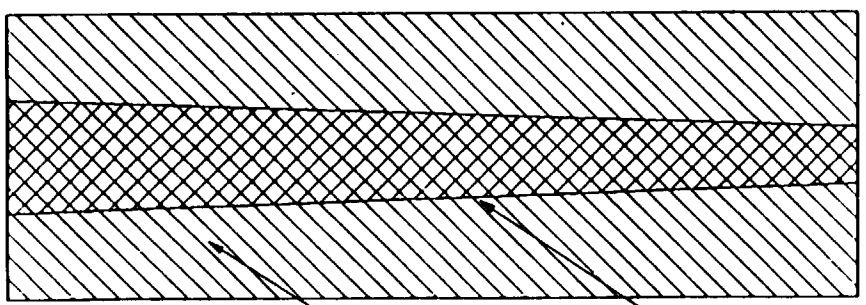

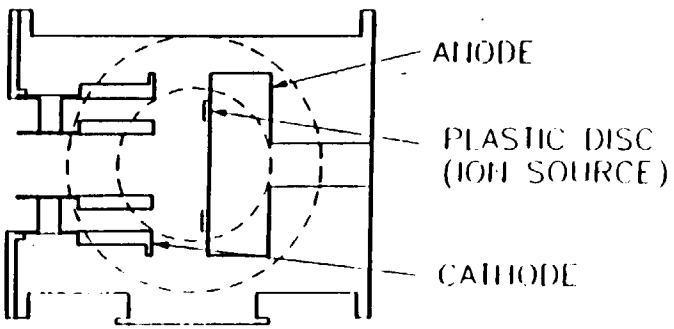

FIG 1

BACKGROUND DENSITY PROFILES

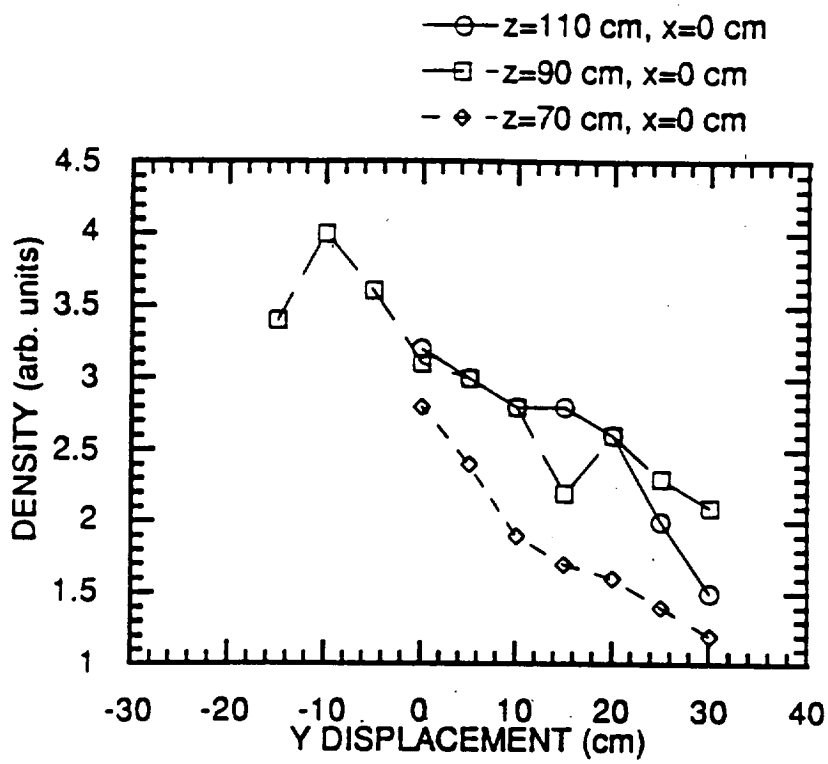

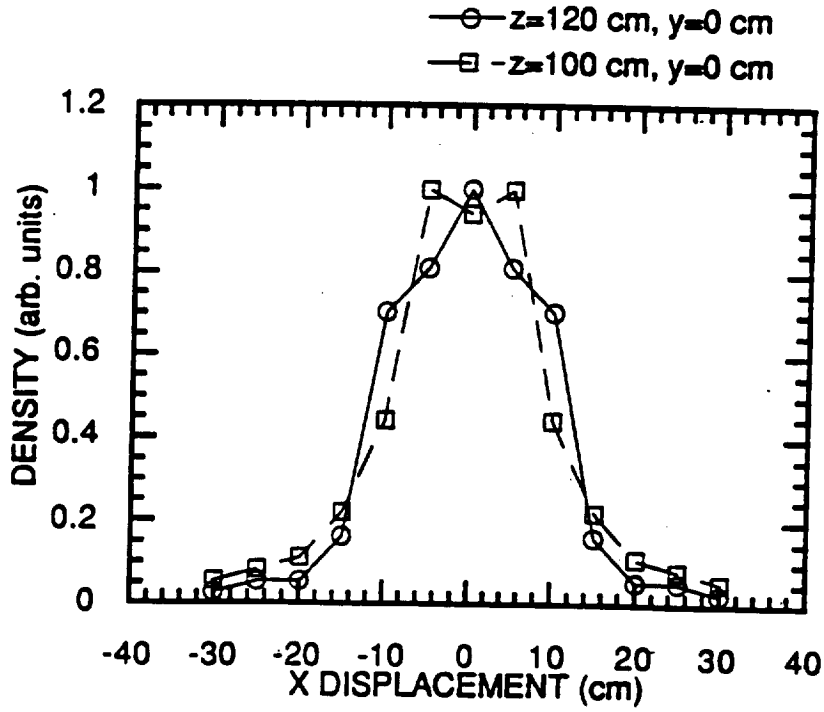

6-12-92

BEAM DENSITY PROFILE AT Z=90 cm

NO VERTICAL FIELD; V=225 kV; LARGE FARADAY CUP

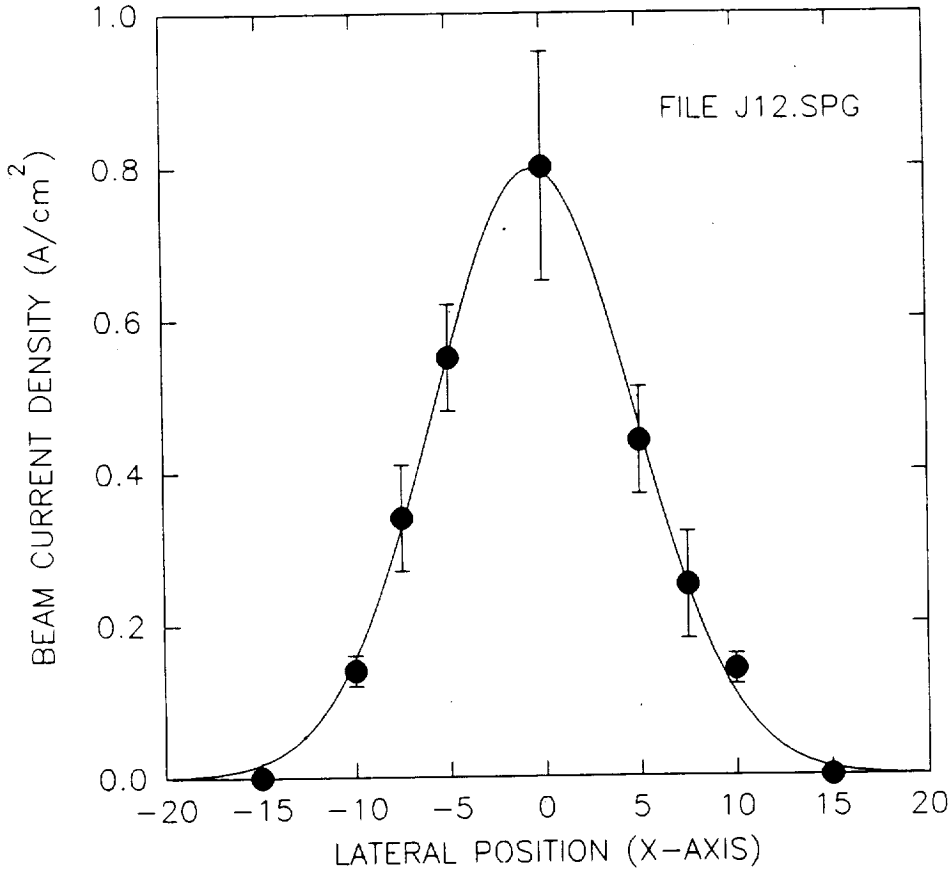

fit curve : $Y = (.797) \times \exp\left\{-\left[\frac{X - .511\ cm}{7.421}\right]^2\right\}$

z measured from collimator opening

VORTICITY TERM

$$[J_{\parallel}]_y = B_0 \int_0^{y_4} \frac{\rho}{B} \frac{d}{dt}\left(\frac{\Omega}{B}\right) dy_{\parallel} = B \int_0^{y_{\parallel}} \frac{\rho}{B} \frac{d}{dt} \left[\nabla \times \langle \bar{v} \rangle \cdot \frac{\bar{B}}{B^2}\right]_y dy_{\parallel}$$

$$\langle \bar{v} \rangle = \frac{v_{beam} \rho_{beam} \hat{k} + v_{plasma} \rho_{plasma} \hat{j}}{\rho_{beam} + \rho_{plasma}}$$

EXPERIMENTALLY:

$$\bar{v}_{plasma} = v_{plasma} \hat{j} \ll v_{beam} \hat{k}$$

$$\rho_{plasma} \simeq \text{constant} \gg \rho_{beam} = \rho_1 \exp\left[-\frac{r^2}{R^2}\right] \exp^{-\frac{(z-vt)^2}{z^2}} \times \exp^{-t/\tau}$$

$$\therefore \langle v \rangle \simeq \frac{v_{beam} \rho_{beam}}{\rho_{plasma}} \hat{k}$$

VORTICITY TERM (cont'd)

$$[J_{\parallel}]_y = \frac{-2V\rho_i}{B} \times \left\{ \frac{2V}{z} \frac{(z-Vt)}{z} - \frac{1}{T} \right\} \exp\left\{ -\frac{(z-Vt)^2}{z^2} \right\}$$

$$\times \frac{x}{R} \exp\left\{ -\frac{x^2}{R^2} \right\} \times \exp\left\{ \frac{-t}{T} \right\} \left\{ C + \int_{-\infty}^{y/R} \exp(-\xi^2) d\xi \right\}$$

$$= {}^{1A}/_{cm^2} \times \text{propagating envelope} \times \text{horiz. profile} \times \text{time} \times \text{vert. profile}$$

$\therefore J_y$ - is linear with V and ρ and inverse with B

- independent of $\rho_{background}$ when $\rho_b > \rho_{beam}$
- antisymmetric in time

$R =$ [illegible] ; $Z =$ [illegible] ; $T = 1/\omega$; $V_{beam} =$ [illegible]

$B =$ [illegible] ; $\rho_{plasma} =$ [illegible] ; $\rho_i =$ [illegible]

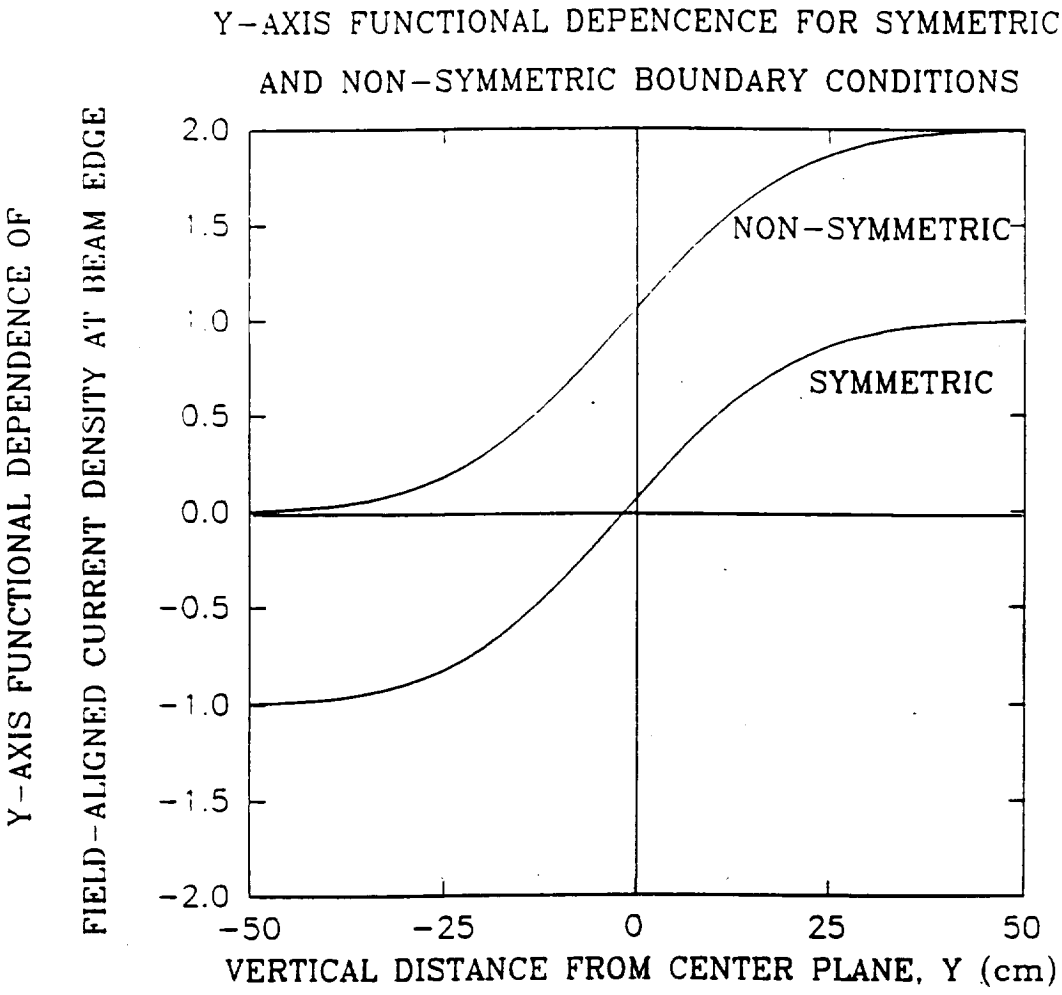
Y-AXIS FUNCTIONAL DEPENCENCE FOR SYMMETRIC
AND NON-SYMMETRIC BOUNDARY CONDITIONS
Y-AXIS FUNCTIONAL DEPENDENCE OF
FIELD-ALIGNED CURRENT DENSITY AT BEAM EDGE
2.0
1.5
1.0
0.5
0.0
-0.5
-1.0
-1.5
-2.0
NON-SYMMETRIC
SYMMETRIC
-50
-25
0
25
50
VERTICAL DISTANCE FROM CENTER PLANE, Y (cm)

FIG. 5.

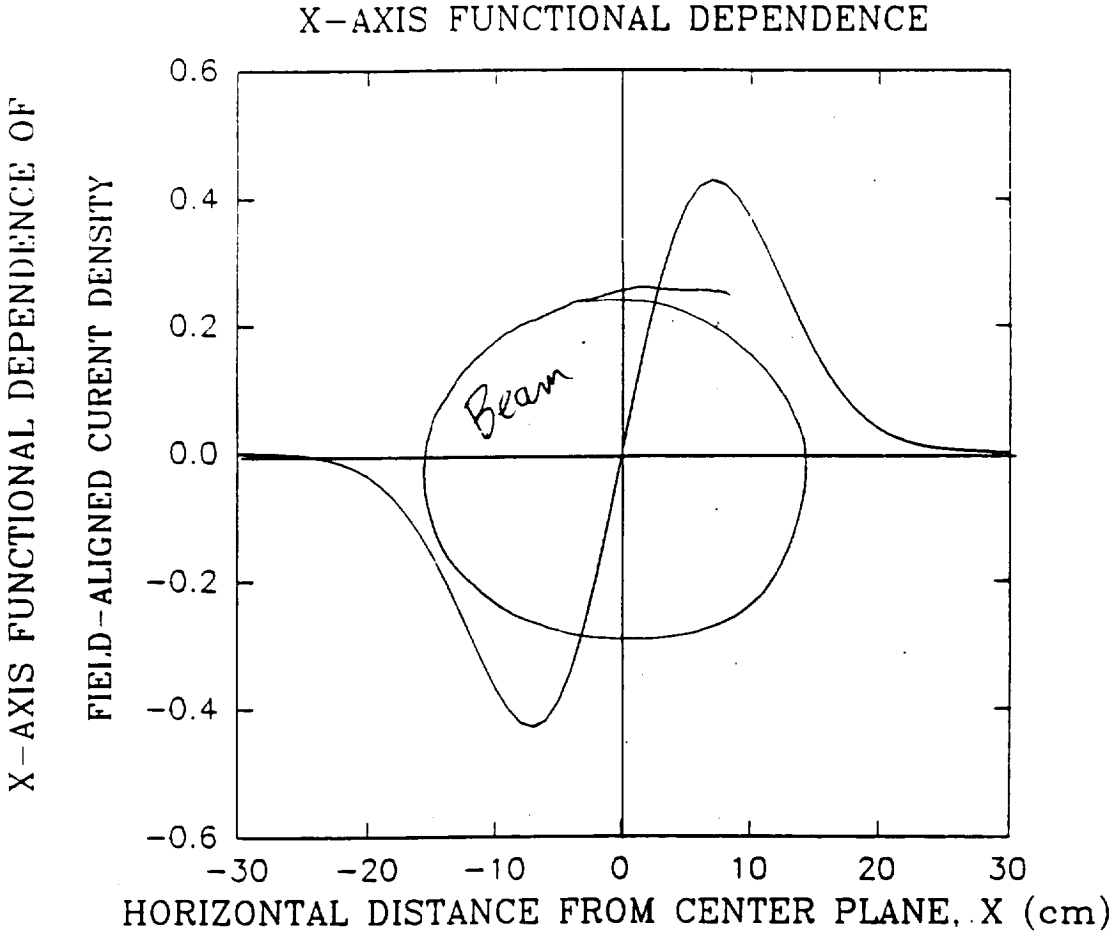
X-AXIS FUNCTIONAL DEPENDENCE
X-AXIS FUNCTIONAL DEPENDENCE OF
FIELD-ALIGNED CURENT DENSITY
0.6
0.4
0.2
0.0
-0.2
-0.4
-0.6
Beam
-30
-20
-10
0
10
20
30
HORIZONTAL DISTANCE FROM CENTER PLANE, X (cm)

3-D VIEW OF THE EARTH'S MAGNETOSPHERE*

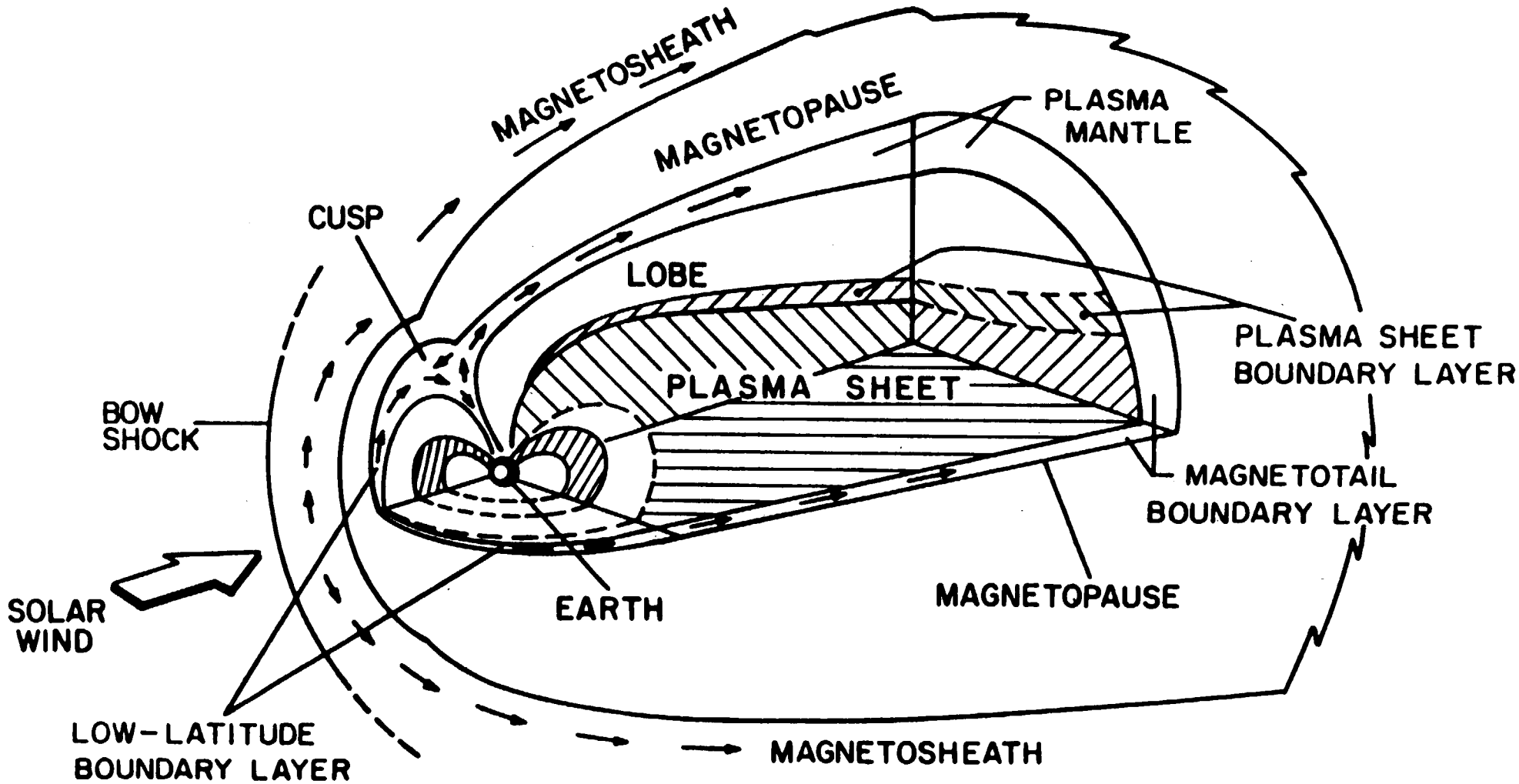

* Figure by T. E. Eastman

FIELD-ALIGNED CURRENT FLOW AT BEAM EDGE FOR

TWO DIFFERENT BOUNDARY CONDITIONS

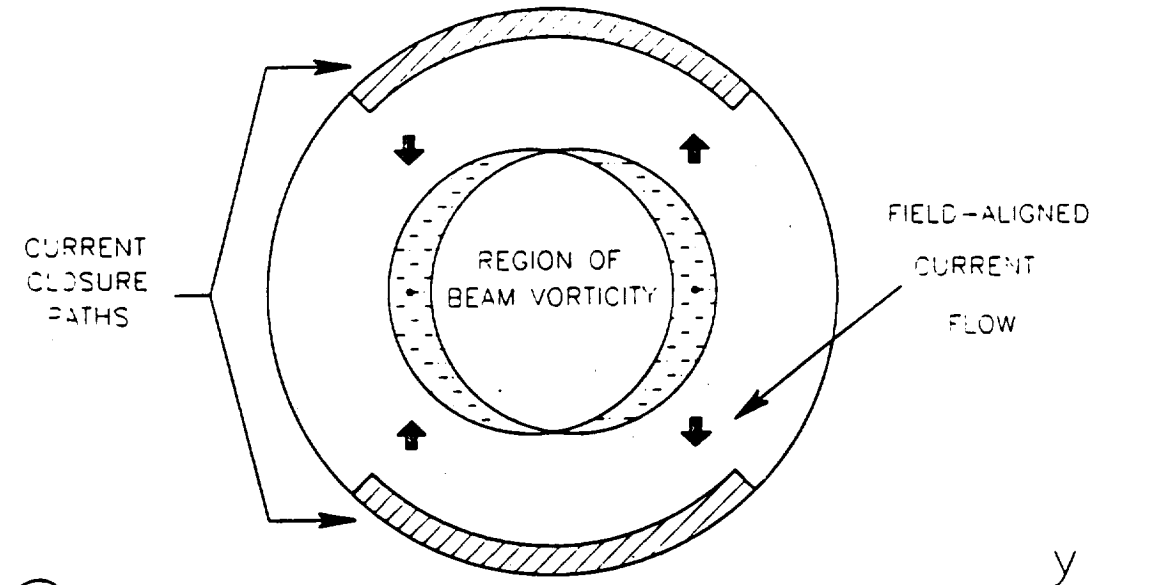

V_{beam}

B_y

SYMMETRIC CLOSURE PATHS

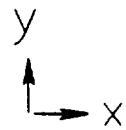

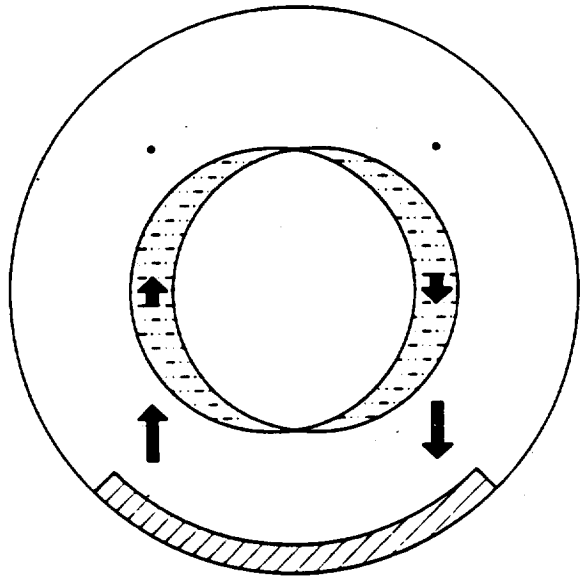

NON-SYMMETRIC CLOSURE PATHS

FIG. 6.

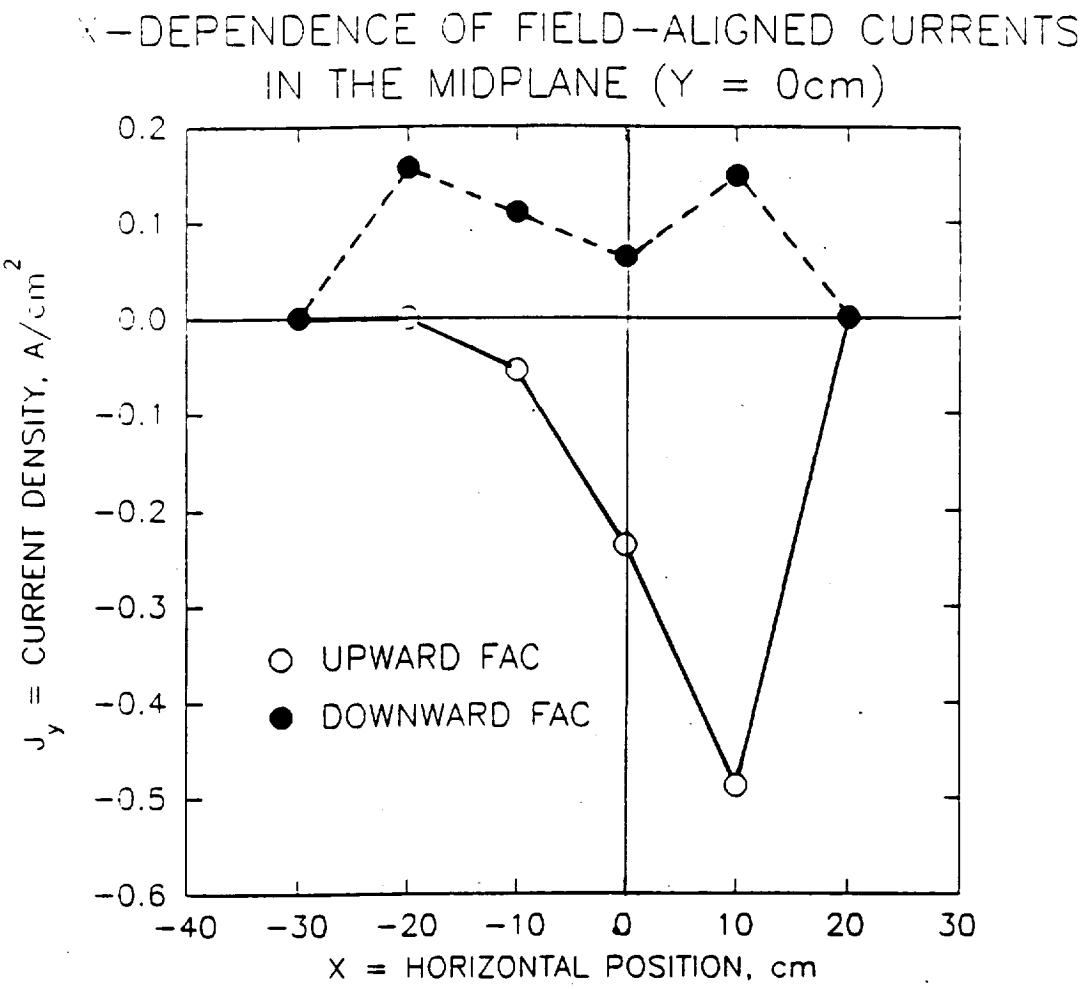

NONSYMMETRIC

MEDIUM ENERGY PLASMA BEAM

- DEFLAGRATION GUN SOURCE RECENTLY TESTED

  $\langle V \rangle \sim 10 \times 10^6$ cm/s

  $J(H^+) = 25 - 800$ A/cm^2

  $\tau = 5$ ms

  (SUITABLE FOR INNER MAGNETOSPHERE STUDIES)

- COMPLETELY SEPARATE FACILITY WILL ALLOW BOTH BEAM SOURCES TO BE USED IN PARALLEL, INDEPENDENT EXPERIMENTS

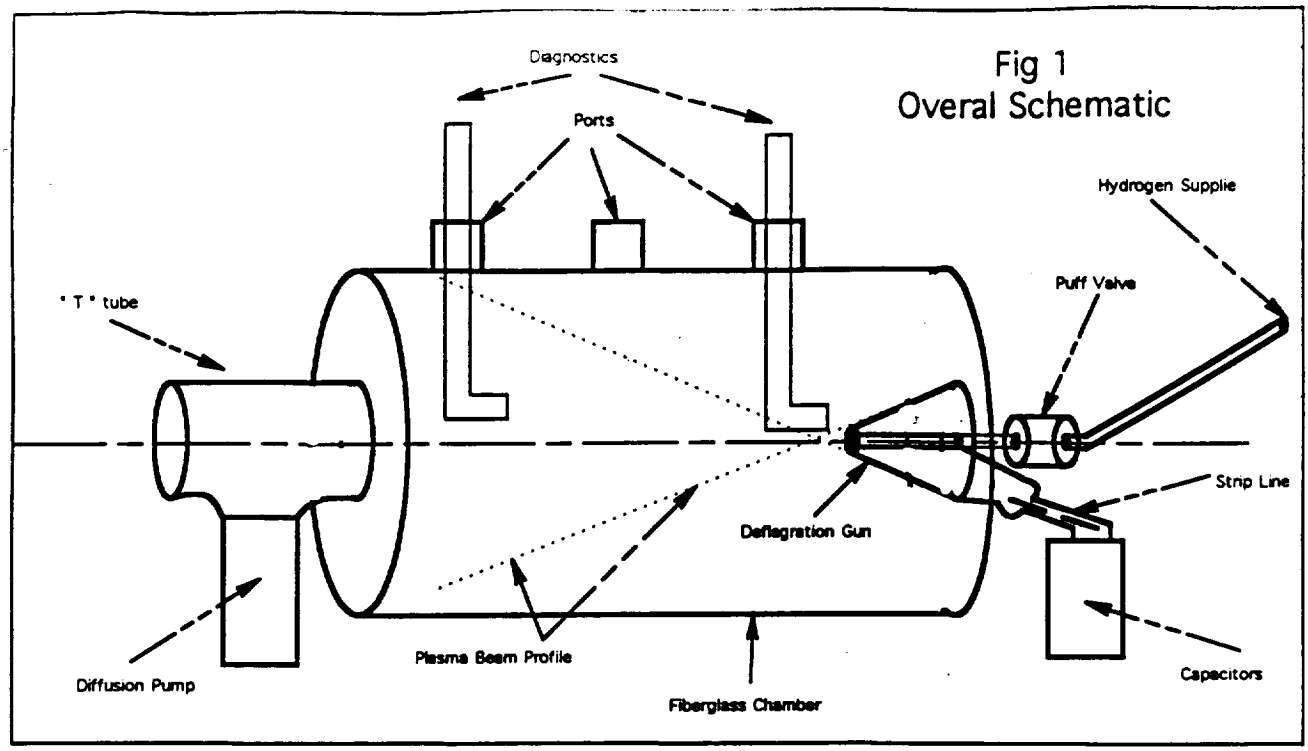

Fig 1
Overal Schematic

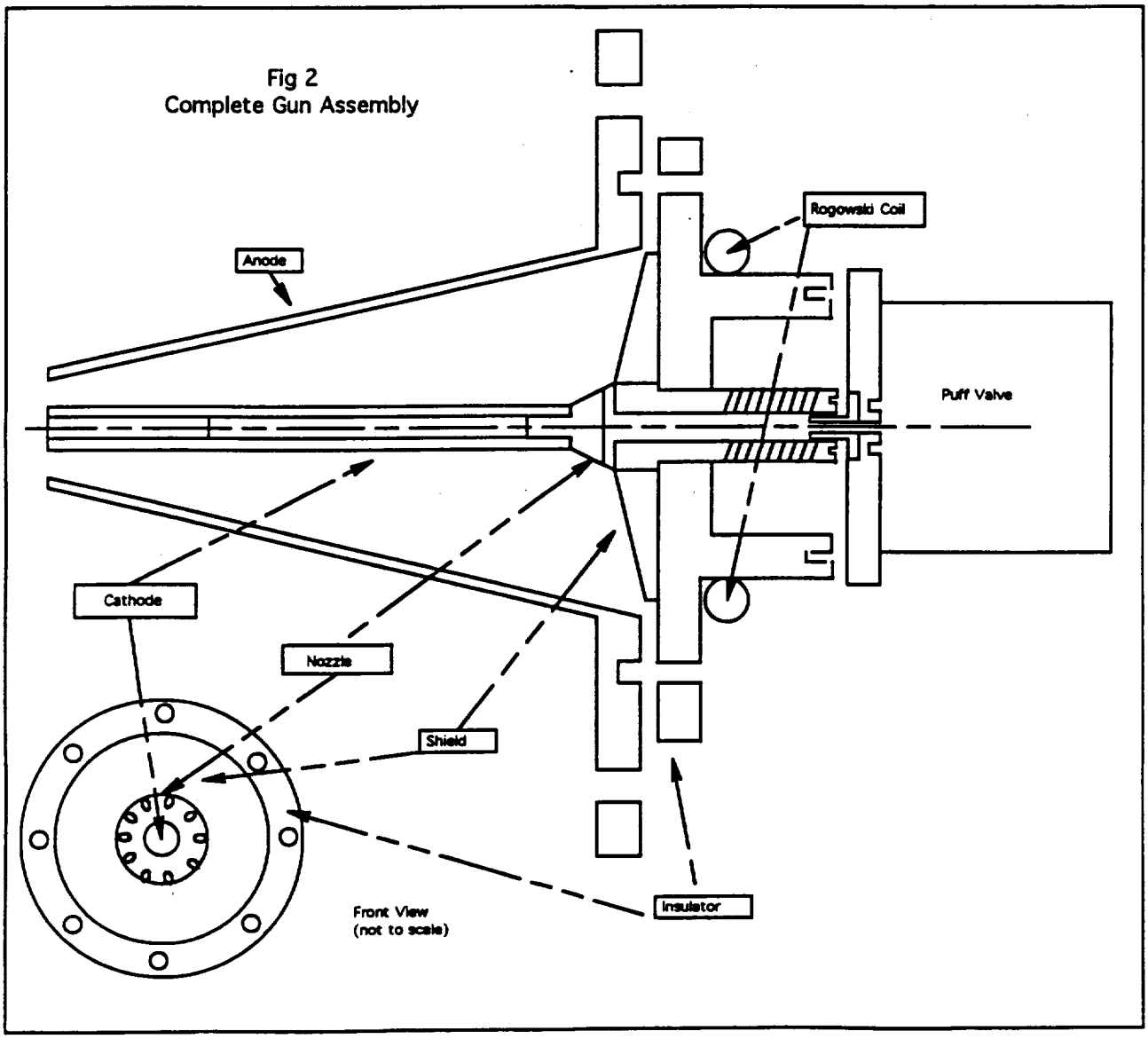

Fig 2
Complete Gun Assembly

Figure 8, Radial Profile

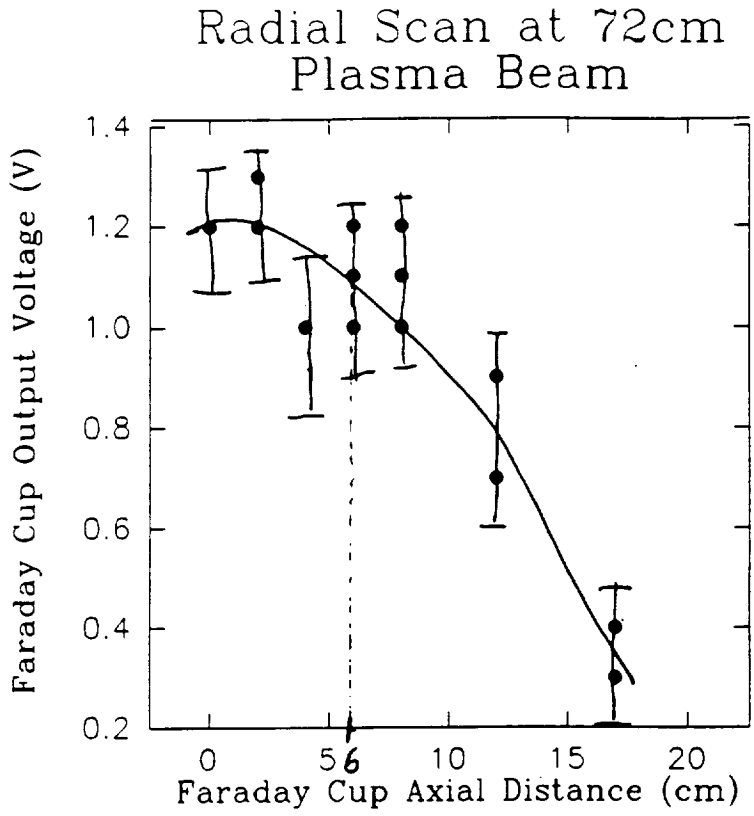

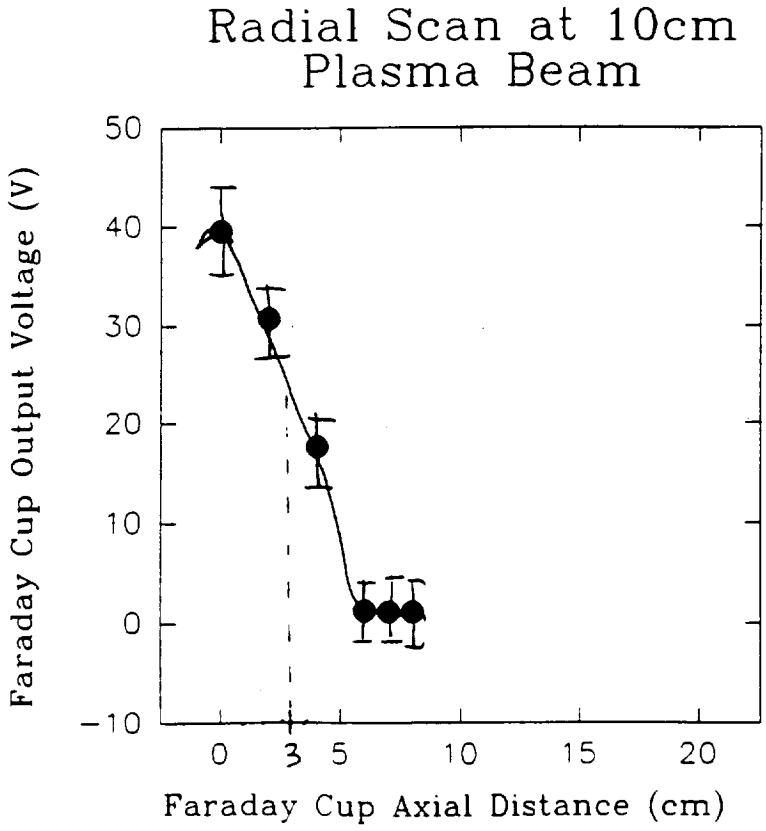

Figure 9, Radial Profile

DIMENSIONLESS COEFFICIENTS

Table 1 compares the magnitudes of these dimensionless parameters for three types of typical laboratory plasma sources to those of the magnetospheric plasma.

The space-plasma parameters are approximately characteristic of the lower-latitude boundaries near the dayside magnetopause, the nightside magnetopause-magnetotail, the central-plasma sheet, and the high-latitude ionosphere (where the field-aligned currents close). For most cases the coefficients R_M , R_I , and L are much greater than unity and can be ignored, unlike the coefficients R_H and R_P and ρ_i/X_o which are of the order of unity and cannot.

It is in these regions of the magnetosphere that the laboratory plasma sources provide a reasonable simulation of the space plasma environment with the additional benefit of flexibility in the experimental parameters, most notably the magnetic field intensity and configuration, plasma density and velocity.

LARGE-SCALE STRUCTURE OF THE MAGNETOSPHERE

The large-scale structure and dynamics of the magnetoplasma is approximately described by MHD models.

However, in boundary layers (see Figure), regions where the particle and field parameters change abruptly, non-MHD processes are important and kinetic effects may dominate:[1]

Magnetosheath
Low latitude boundary layer
Plasmapause
Magnetosphere-ionosphere
Polar-cusp zone

These boundary layers play a key role in the magnetospheric energy-transfer processes[2] even though they comprise a small portion of the total magnetospheric volume.

---

[1] Vasyliunas, V. M., Large scale models of the ionosphere/magnetosphere/solar wind system-a unifying principle, Modeling Magnetospheric Plasma, T. E. Moore and J. H. Waite, Jr., Editors, AGU Monograph # 44, p. 33, 1988.

[2] Rostoker, G. and Eastman, T. E., "A Boundary Layer Model for Magnetospheric Substorms", J. Geophys Res. 92, 12,187(1987).

MAGNETIC DIFFUSION IN HIGH BETA PLASMAS

- HIGH BETA EXPERIMENTS REPORT ANOMALOUSLY FAST MAGNETIC DIFFUSION IN GUN PLASMAS , ION BEAMS, LASER PLASMAS, ACTIVE SPACE PLASMAS

- GENERALIZED OHM'S LAW AND MAXWELL'S EQUATION

$$\mathbf{E} = -\frac{\mathbf{v}\times\mathbf{B}}{c} + \frac{\mathbf{J}}{\sigma} + \frac{\mathbf{J}\times\mathbf{B}}{nec} - \frac{\nabla P}{n} + \frac{m}{ne^2}\frac{\partial \mathbf{J}}{\partial t}$$

$$-\frac{1}{c}\frac{\partial \mathbf{B}}{\partial t} = \nabla \times \mathbf{E} \qquad \Rightarrow \text{A MAGNETIC DIFFUSION EQUATION}$$

- SCALED ANALYSIS OF THE MAGNITUDE OF EACH TERM IN OHM'S LAW GIVES, (NORMALIZED TO THE $\frac{\mathbf{v}\times\mathbf{B}}{c}$ LORENTZ FORCE TERM)

$$\nabla \rightarrow \frac{1}{x_o} \qquad v \rightarrow v_o \qquad \frac{\partial}{\partial t} \rightarrow \frac{1}{t_o}$$

$$\frac{1}{R_{ohmic}} = \left(\frac{c}{\omega_e}\right)^2 \frac{\nu_{ei}}{x_o v_o} \qquad \frac{1}{R_{hall}} = \left(\frac{c}{\omega_e}\right)^2 \frac{\Omega_e}{x_o v_o} = \frac{1}{\beta_d}\frac{\rho_i}{x_o}$$

$$\frac{1}{R_{pressure}} = \frac{v^2_{te}}{\Omega_e x_o v_o} = \frac{\beta_t}{\beta_d}\frac{\rho_i}{x_o} \qquad \frac{1}{R_{inertial}} = \left(\frac{c}{\omega_e}\right)^2 \frac{1}{x^2_o}$$

SCALING (contd)

Below 150 km (ionosphere) the plasma is weakly ionized, the neutral density is high, and charged particle-neutral collisions determine the conductivity. In this region electrons are magnetized and the ions are dragged across the B field by neutral winds in the upper atmosphere. Thus, the species-dependent anisotropic-conductivity must be considered:

$$\frac{\underline{J}}{\sigma} \rightarrow \frac{\underline{J}_{||}}{\sigma_{||}} + \frac{\underline{J}_{\perp}}{\sigma_{\perp}}$$

$$R_M^{-1} \rightarrow \frac{c^2}{4\pi\sigma X_o V_o}$$

where σ is the parallel or perpendicular (Pederson and Hall) conductivities for the electrons and ions. At 150 km altitude: $n_o = 10^{10}$ cm^{-3}, $n_i = n_e = 10^4$ cm^{-3}, $T_i = 0.1$ eV, $T_e = 1$ eV

$$\sigma_{||\alpha} = \frac{ne^2}{m_\alpha \nu_\alpha}, \quad \sigma_{\text{Pederson}\alpha} = \frac{\sigma_{||\alpha}}{1+(\Omega_\alpha/\nu_\alpha)^2}, \quad \sigma_{\text{Hall}\alpha} = \frac{\sigma_{||\alpha}\,\Omega_\alpha/\nu_\alpha}{1+(\Omega_\alpha/\nu_\alpha)^2}$$

	$\sigma_{||}$	σ_{Pederson}	σ_{Hall}
σ_e	$\sim 6 \times 10^9$	$\sim 6 \times 10^5$	$\sim 6 \times 10^9$
σ_i	$\sim 2 \times 10^9$	$\sim 2 \times 10^7$	$\sim 2 \times 10^9$

FIELD-ALIGNED CURRENTS

VORTICITY TERM :

$$\nabla \times \bar{v} = -\hat{j}(\partial_z V_x) + \hat{k}\,\partial_y V_x$$

$$\nabla \times v \cdot B \rightarrow (\partial_y V_x) B_z$$

$$J_{\parallel} = B \int_0^{\ell_{\parallel}} \frac{\rho}{B} \frac{d}{dt}\left[\nabla \times \bar{v} \cdot \frac{\bar{B}}{B^2}\right] d\ell_{\parallel}$$

USE: $\partial V_x / \partial y \rightarrow V_x(t)/\Delta y$

can vary $\dfrac{\partial V_x}{\partial y}$ by apertures increase ρ

$$J_{\parallel} = \frac{\rho \ell_{\parallel}}{B \Delta y} \frac{dV_x}{dt} = \frac{\rho \ell_{\parallel}}{B \Delta y}\left(-\frac{V_x}{\tau_s}\right)$$

FOR: $B = 0.03\,T$, $\ell_{\parallel} = 0.3\,m$, $\Delta y = 0.05\,m$,

τ_s(DPB) $\approx 50\,\mu s$ $= 1.6\times10^{-9}\, n_p/T^{3/2} \ln\lambda$

τ_s(IPB) $\approx 1000\,\mu s$ $= 1.7\times10^{-4}\, n_p/T^{3/2} \ln\lambda$

$\Rightarrow$ $J_{\parallel} \approx 10\ A/cm^2$

FIELD-ALIGNED CURRENTS

MAGNETIC-FIELD GRADIENT TERM:

$$J_{\parallel} = B\int_0^{\ell_{\parallel}} \frac{2}{B^2}\,\bar{J}_{\perp}\cdot\bar{\nabla}B\;d\ell_{\parallel} \;\rightarrow\; \frac{2}{B}\,J_{\perp}\,\nabla B\,\ell_{\parallel}$$

PAST UCI EXPERIMENTS HAVE MEASURED COMPONENTS OF $\bar{J}_{\perp}$:

$$\bar{J}_{\perp} = \bar{J}_D + \bar{J}_I$$

	DPB	IPB
J_D	$20\,A/cm^2$	~0
J_I	$2\,A/cm^2$	$5\,A/cm^2$

FOR $\bar{\nabla}B \approx 50\ G/cm$:

$$\Rightarrow \quad J_{\parallel} \approx 3\,A/cm^2$$

FIELD-ALIGNED CURRENTS

DENSITY-GRADIENT TERM:

$$J_{\parallel} = B \int_0^{\ell_{\parallel}} \frac{1}{\rho B} \bar{J}_I \cdot \nabla\rho \, d\ell_{\parallel} \rightarrow \frac{J_I}{\rho} \nabla\rho \, \ell_{\parallel}$$

USING WALL-MOUNTED PLASMA-GUN ARRAYS:

$$\nabla\rho \sim 1.6 \times 10^{-12} \text{ gm/cm}^4 \qquad \left(\nabla n \sim 10^{13} \text{ cm}^{-3}/10\text{cm}\right)$$

$$\Rightarrow J_{\parallel} \simeq 2.5 \text{ A/cm}^2$$

Attachment 2.

University of California, Irvine, internal report on
"Characterization of a deflagration plasma gun,"

Characterization of a deflagration plasma gun

N. M. Melville (summer REU), F. J. Wessel,
W. W. Heidbrink, J. Manson, and S. Drum
University of CA, Department of Physics,
Irvine CA 92717-4575
Aug. 23, 1992

Abstract

A plasma deflagration gun has been constructed for use as a pulsed source of high density, high velocity plasma. The gun has seen a preliminary run through wherein its characteristics support active plasma production via the deflagration process. The charging voltage of -8.03 kV has produced a 200 kA current pulse maximum, with a risetime of 4.4 μs. There is evidence of geometric focusing, and plasma current densities ranging from 26.4 A/cm^2 off focus to 872.2 A/cm^2 near focus. Average plasma velocities have been measured to be, 1.4x10^7 cm/s. Total number of particles/pulse were calculated to be, 3-5 x10^{17}.

Introduction

Although high energy plasmas have been created using MARX generators in ongoing UCI experiments, the need has arrived for a lower velocity, higher density plasma pulse. This plasma pulse is necessary to simulate field-aligned currents in the earth's magnetosphere due to the solar wind. The deflagration mode is appropriate for modeling this phenomenon as the velocities of the solar wind are comparable to that created by the deflagration gun. Solar wind velocities approaching 5x10^6 cm/s are comparable to the deflagration plasma velocities of 10^6 - 10^8 cm/s.

As first developed by Cheng[1], plasma deflagration guns provide high density, 10^{14} cm^{-3}, high velocity, >10^8 cm/s, at reasonable thermal energy, 10 keV. The deflagration process can be summed up in a quote from Cheng: " When a combustible mixture is ignited from one end of a prefilled tube, two types of flames can be observed. If the tube is completely sealed during the process, a strong explosive fast wave will be propagated from one end of the tube to the other. The velocity of the propagation usually has a fixed value . This is known as a detonation. On the other hand, when the mixture is ignited from the open end of a prefilled tube, a slow wave is propagated from one end to the other , whereupon the byproduct of the combustion is exhausted in the opposite direction from the combustion wave, through the open end. This is known as deflagration."

The design and performance of our gun are referenced to Dr Cheng's work, with several modifications. The pre-expansion gas cavity was eliminated in favor or ten-radial holes at the breach of the cathode electrode. The quartz insulator, used to hold-off the high voltage, has been replaced with polyurethane which proved to be a dependable inexpensive replacement; a conical Pyrex disk was epoxied to the vacuum discharge surface of the insulator to prevent surface carbonization after gun firing which would otherwise develop.

Experimental Apparatus

Firing Procedure

The overall schematic of the experiment is illustrated in Fig.1. The fiberglass chamber is pumped down to $3x10^{-5}$ torr. A voltage difference of -8kV is applied between the gun anode and cathode by a charged capacitor. The gun is triggered when hydrogen gas at approximately 55 psi, is compressed and then injected into the gun by a puff valve. The hydrogen gas expands into the gun cavity through ten radial holes in the breech of the gun cathode. Electrical breakdown occurs through the hydrogen gas ionizing it. The plasma is then accelerated by self-generated electrodynamic forces and ejected out the muzzle into the chamber.

Vacuum system

The vacuum chamber is roughly 2-m long and 1-m diameter with two aluminum flanges on each end of the chamber (c.f., Fig 1). The chamber is made of fiberglass because of its low cost and relatively low magnetic permeability compared to steel. It is also a good insulator which provides little interaction with desired events within the tank. Ten access ports, each 2-inch diameter, are positioned along the chamber exterior, 30 cm from each other, with 2 on the top 2 on the bottom and three on either side of the chamber. On one end of the chamber is a large metal"T" tube with one end used as a view port and the other two openings as a flow path for evacuating the the chamber with an oil-diffusion pump. The diffusion pump must operate at pressures below < 500 μtorr, thus there is another port through the aluminum flange for rough pumping the chamber down to this level. The rough pump is also used to pump the exhaust of the diffusion pump. The flow path of the roughing pump is controlled by two compressed air valves.

The chamber will normally rough down to 500 μtorr in 1-2 hours. Then the diffusion pump is employed pumping the chamber down to $5x10^{-4}$ torr. A lower initial pressure is limited by outgasing inside the chamber, or perhaps, a slight leak. Leaks are checked by spraying isopropanal on the chamber seals; all seals are of the o-ring type or Wilson seals. If there is a leak the pressure will go up sharply. If the pressure does not go up then there is still some outgasing. The outgasing lasts 15 min - 24 hours, with an ultimate pressure of approximately, $2x10^{-5}$ torr. After firing the gun the pressure jumps to 100 μtorr and then pumps down to base pressure ($2x10^{-5}$ torr) within two to three minutes.

Deflagration Gun

An illustration of the plasma gun is shown in Fig 2. The anode barrel is a stainless steel cone with a 6 degree half angle. The apex has been truncated to make the muzzle. The barrel is 12-inch long and 4-inch diameter at the breech. The muzzle is 1.6-inch diameter. The cathode consists of a stainless steel rod 1/2-inch diameter and 11.75-inch long. Welded to the breech of the rod is the gas injection nozzle. The nozzle consists of ten evenly spaced 3/16-inch diameter holes drilled radially at the beginning of the taper. The holes intersect at the rod center where a 0.327-inch diameter hole is bored out the back axially. This tube is the hydrogen transport cavity.

The cathode is attached to an insulator disk with a 1.0 inch nut. The insulator is the only physical connection between the anode and the cathode, thus the vacuum side of the insulator surface is susceptible to voltage breakdown. To prevent voltage breakdown, a Pyrex tapered disk is epoxied onto the face of the insulator surrounding the cathode. The Pyrex resists carbonization.

The cathode is screwed onto the insulator, and the insulator is then attached to the cone with four bolts. The cone is screwed down to the aluminum flange on the chamber. Thus the chamber is at the same potential as the anode.

Gun Power Supply

The gun center electrode is charged in the range 2-8 kV negative by attaching two, 60 μF Capacitors in parallel rated at 10 kV. The leads to the anode and cathode are connected by a short (30-cm long) parallel-plate stripline. The stripline is constructed from a 30 cm x 30 cm printed circuit board which is soldered to four pieces of 0.01-inch thick shim stock. The stripline has succeeded in carrying >200 kAmps for >50 shots. Capacitor bank charging takes four to five minutes.

Gas injection

Gas injection is provided by means of a puff valve (Fig. 3), which operates using diamagnetic repulsion.[2] A capacitor (Fig.4) is discharged into a 90-μH coil, creating a magnetic field that repels an aluminum ring resting above the coil. This ring is allowed to accelerate through a distance of 7 mm, achieving a large velocity before striking a nylon poppet. The poppet is then driven off an o-ring, rapidly opening the valve and permitting the flow of gas.

The coil drive voltage ranges between 500-600 V. At a charging voltage of 506 volts, the puff valve discharging pulse reaches a maximum current of 580 A in 250 μs. The puff valve is attached to the gun cathode by a brass cylinder milled to fit inside the cathodes gas-flow cavity. A vacuum seal is made with an oversized o-ring around the brass cylinder up against the cathode o-ring grove. Then comes a washer as a spacer and another o-ring that fits tightly around the brass cylinder. The o-rings are compressed, and the puff valve is supported by bolting it onto the insulator with nylon screws. Compressed hydrogen gas is piped into the puff valve with plastic tubing and Wilson seals. The gas-supply line was evacuated to 3×10^{-5} torr before filling.

Diagnostics

Current Detection

Gun current is measured with a Rogowski coil. The magnetic induction from the current running through the gun induces a voltage potential at opposite ends of an inductor looped around the current path. The Rogowski coil output voltage is,

$$V_{out} = (2NA/r)\, I/t$$

where, V_{out} = the output voltage, A = area enclosed by a single turn of the inductor (0.785 cm^2), N = # of turns (36), I = maximum current, t= risetime, r= Radius of loop. The unintegrated Rogowski probe sensitivity as function of current frequency is shown in Fig. 5; the gun operating frequency is between 30 and 50 kHz. As shown in the data, the Rogowski coil of 36 turns has a constant output voltage within this range.

The Rogowski coil was recalibrated with a 10 μs integrator. The calibration was done with a terminated Pearson probe in series with the integrated Rogowski coil, around one of two leads to the gun anode. The gun was fired at 2 kV. The integrated Rogowski Coil was calibrated to 23.164 kA/V at 26 kHz. The final frequency of the gun was 47.6 kHz when the stripline was employed. The integrated Rogowski coil was then placed around the insulator ring to measure the current flow through the cathode (Fig 2).

Faraday Cup

Faraday cups were used to measure the plasma-current density, time-of-flight plasma velocity, as well as the beam radial profile. A faraday cup is shown in figure 5. The cup consists of a small graphite collector cup surround by a brass shield. The center electrode is biased to a negative voltage (-100 volts) and the outer shield is ground potential, the negative bias unneutralizes the plasma flow to measure the ions. The only path by which plasma can be collected is through a small hole in the brass shield. The hole collimates the plasma as well as allows the cup sensitivity to be changed. The Faraday cup output voltage as a function of time is proportional to the amount of current flowing through the hole in the shield. The plasma current density is calculated by the following:

$$J = \text{Area of hole} \times V_{out} / R_{cup} .$$

In this experiment , R_{cup} = 50 ohms and A =0.34 mm^2.

The plasma front velocity, and average velocity can be measured by using multiple cups at varying distances from the gun. This gives time-of-flight measurements that easily be translated into velocities by measuring the distances between the cups. Average velocity is calculated by measuring the time it takes for each cup to read the averaged maximum current pulse; the front velocity is measured at the beginning of each cup's current pulse.

The plasma density is calculated from:

$$n = J/ev$$

where, e= charge of electron, v= plasma velocity.

The total streaming energy can be extrapolated from the following equation:

$$E = 0.5 N m_H V^2$$

where, N= # of ions in plasma beam, m_H= mass of hydrogen ions, V= average velocity of plasma. The beam profile and divergence can also be measured by positioning the Faraday cup in varying radial positions and axial distances from the gun.

Calorimeter

In an attempt to measure the total amount of energy in the plasma beam a calorimeter was constructed to collect the plasma and convert it's streaming energy into thermal energy (Fig 6). The thermal heating is then measured by the change in resistance of a precision thermistor (YSI 44006 10,000 OHMS @25C) glued onto the side of the calorimeter with a mixture of epoxy and finely pulverized silver powder.

The calorimeter is made from 150 grams of copper in the form of a cone. The copper is 1/32 of an inch thick and is hand hammered into the shape of a right circular cone. The base diameter of the cone is 3 inches and it's length is 5.75 inches. The cone is suspended by Kevlar thread from a fiberglass circuit board. The board is attached to a rod which feeds the thermistor electrical leads outside the chamber to an ohm meter. The energy is related to the change in temperature as follows:

$$E = C_V \times m \times \Delta T$$

where, C_V = specific heat, m = mass, ΔT = change in temperature.

The amount of energy stored (E), in the capacitors is calculated from:

$$E = 0.5CV^2$$

where, C = 120 μFd , V = charging voltage. The total stored energy is 3.8 kJ at 8 kV. If 80% of the stored capacitor energy is measured, then ΔT should be 50 C°.

Preliminary Results-

The time-dependent data is collected by a 400 Ms/sec 100 MHz GOULD 4074 four channel digital storage scope. Measuring the voltage on the gun capacitors is done with a multimeter attached to a high voltage probe with a 1000/1 voltage divider.

The gun provided 200 -211 kAmps at 47 khz for over 50 shots.(see Fig. 7) The current risetime of the gun can is calculated from the following:

$$t = \pi/2(LC)^{0.5} = 4.4\ \mu s$$

Thus, for the parameters of the experiment,

$$L = 0.065\ \mu H.$$

The maximum ΔT measured 2 inches downstream from the gun with the calorimeter was 12 C°. This translates into 0.75 kJ, which is 20 % of the total energy stored in the capacitors (3.8 kJ). It is possible that plasma bounced out of the calorimeter before its kinetic energy was absorbed.

The radial beam profile was measured at two downstream distances from the muzzle of the gun. First from port #8, 72 cm from the gun and second from port # 2 which is 10 cm from the gun. The expected profile was a converging cone coming to a focus at 15.25 cm with a 6° half-angle divergence. At 10 cm from the gun the expected radial plasma dimension was 3 cm and at 72 cm the expected radial dimension was 6 cm. The data in Figures 8 & 9 confirm this profile and the gun seems to provide a geometric focus.

The plasma current densities were calculated from the faraday cup voltage output, located at r = 0 on the gun axis. The gun the current density is:

$$J = 1.2\ V/(50\ \Omega \times 9.08\times10^{-4}\ cm^2) = 26.4\ A/cm^2$$

at 72 cm and at 10 cm:

$$J = 39.6\ V/(50\ \Omega \times 9.08\times10^{-4}\ cm^2) = 872.2\ A/cm^2$$

The time of flight for the beam front to travel 36 cm was measured to be 2 μs. The average was measured to be 2.5 μsec (see fig 10). This translates into:

$$V_{average} = 1.4\times10^{7}\ cm/s$$

$$V_{front} = 1.8\times10^{7}\ cm/s$$

Plasma densities are calculated at the same two downstream distances as, n = J/ev, J = current density, e = 1.6×10^{-19} C, v = velocity. The density is:

$$n = (26.4)/1.6\times10^{-19} \times 1.4\times10^{7} = 1.2\times10^{13}\ cm^{-3}$$

at 72 cm from the gun and at 10 cm downstream distance

$$n = (872.2)/1.6\times10^{-19} \times 1.4\times10^{7} = 3.9\times10^{14}\ cm^{-3}$$

The total number of particles is calculated from, N = n Avt , where n = # density, A = cross sectional beam area, v = velocity, t = pulse duration.

At 72 cm from the gun:

$$N = (1.2\times10^{13})\ (\pi\ [8cm]^2)\ (\ 1.4\times10^{7} cm/sec\ )\ (10\ \mu sec)$$

$$= 3.4 \times 10^{17}\ particles$$

At 10 cm from the gun:

$$N = (3.9\times10^{14})\ (\pi\ [3cm]^2)\ (\ 1.4\times10^{7} cm/sec\ )\ (3\ \mu sec)$$

$$= 4.6 \times 10^{17}\ particles$$

The total energy is calculated from, $E = 0.5\ Nm_H V^2$, V = 5.6×10^{6}cm/s, m_H = 1.6×10^{-24} g, N = total # of particles. At 72 cm from the gun :

$$E = 0.5\ (3.4\times10^{17})\ (\ 1.6\times10^{-24}\ g)(\ 1.4\times10^{7} cm/sec\ )^2$$

$$= 5.33 \times 10^{7}\ ergs\ *\ 10^{-7} joules/erg = 5.33\ joules$$

At 10 cm from the gun :

$$E = 0.5\ (4.6\times10^{17})\ (\ 1.6\times10^{-24}\ g)(\ 1.4\times10^{7} cm/sec\ )^2$$

$$= 7.21 \times 10^{7}\ ergs\ *\ 10^{-7} joules/erg = 7.21\ joules$$

The resulting energy in the plasma beam as calculated above is 5.33 -7.21 joules. This is a troubling number, as the calorimeter energy calculation, which measured only 20% of the stored energy, was that of 750 joules. It was hoped that the faraday cup was a better instrument with which to measure the energy in the plasma, however this does not seem to be the case. The calorimeter may have been able to gather the energy of both ionized and unionized particles, while the faraday cup only calculates the energy by

measuring the energy in the charged ions. If the gas is only 10% ionized, then it is possible that the faraday cup is reading only 10% of the energy in the gas-plasma system. Thus the energy measured by the faraday cups being equal to 53.3 - 72.1 joules. This is close to that measured by the calorimeter. However this assumes that most of the energy is actually in the unionized gas. Whether this is actually the case still remains to be seen

Future

The deflagration gun should have another radial-scan profile measured at a further downstream location to verify energy partitioning. Vertical magnetic field coils placed around the chamber will be constructed to mimic the earth's magnetosphere in the tank. Plasma-strip guns will be installed at the bottom of the chamber to produce a background plasma which simulates the conditions in the earth's extreme upper atmosphere.

References

1. Cheng, D.Y.; "Plasma deflagration and the properties of a coaxial plasma deflagration gun," Nuc. Fusion 10, (1970).
2. Kriesel, J.; Prohaska, R.; and Fisher, A. ,et. al.; "Simple Fast Puff Valve," Rev. Sci. Inst. 62, (1991).

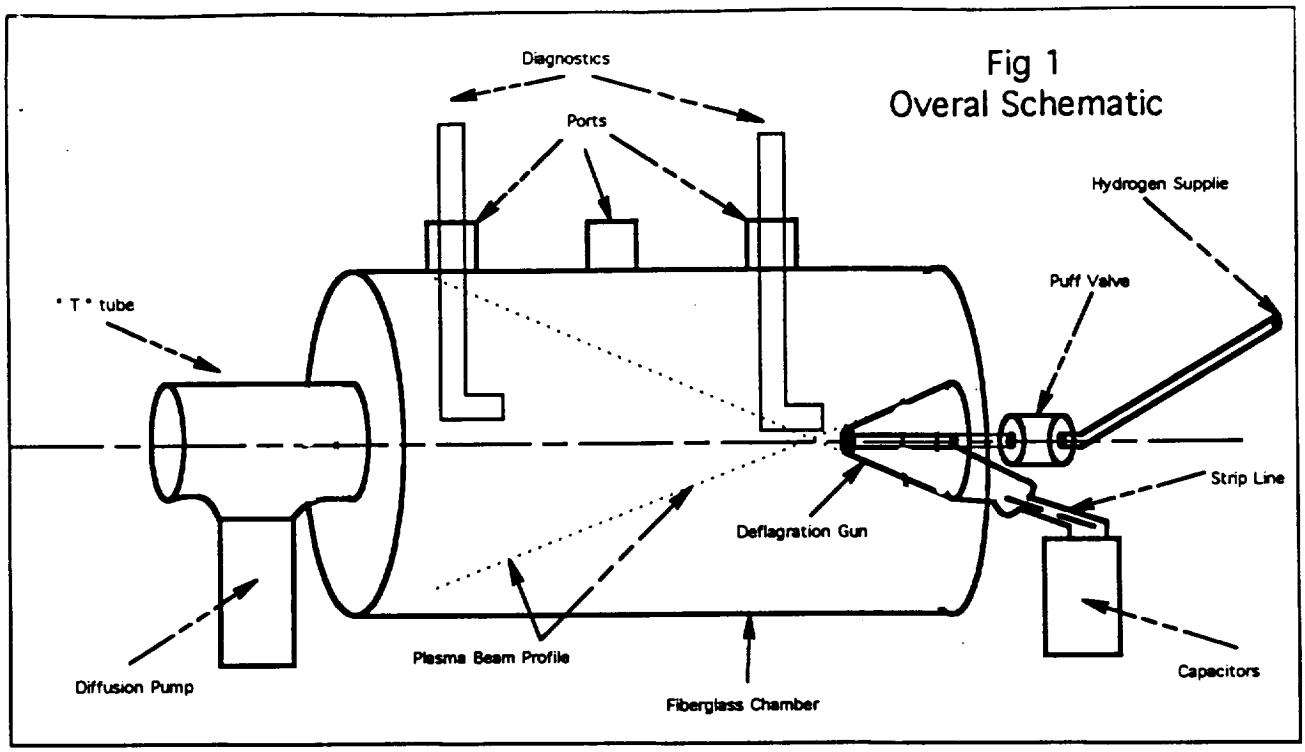

Fig 1
Overal Schematic

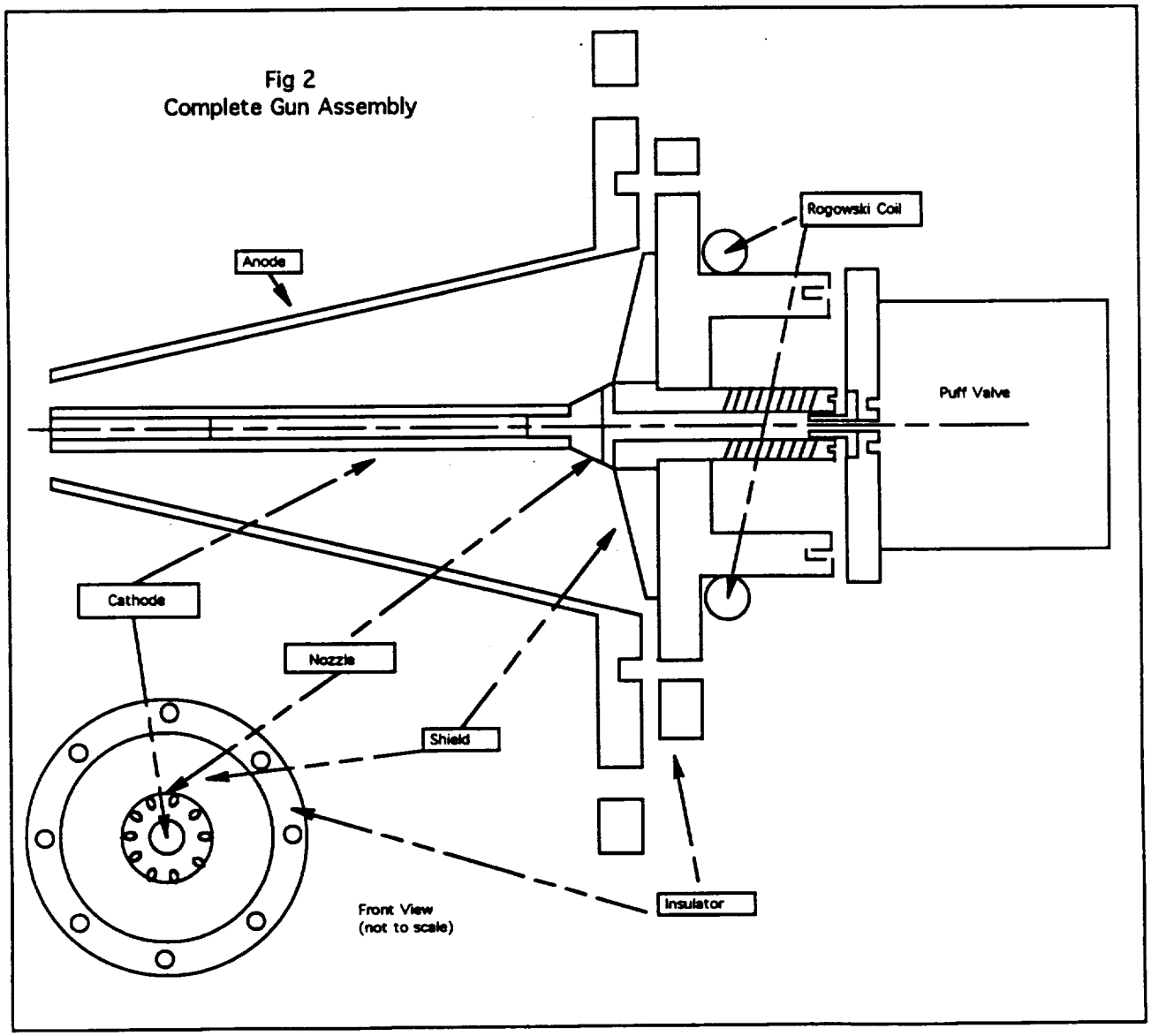

Fig 2
Complete Gun Assembly

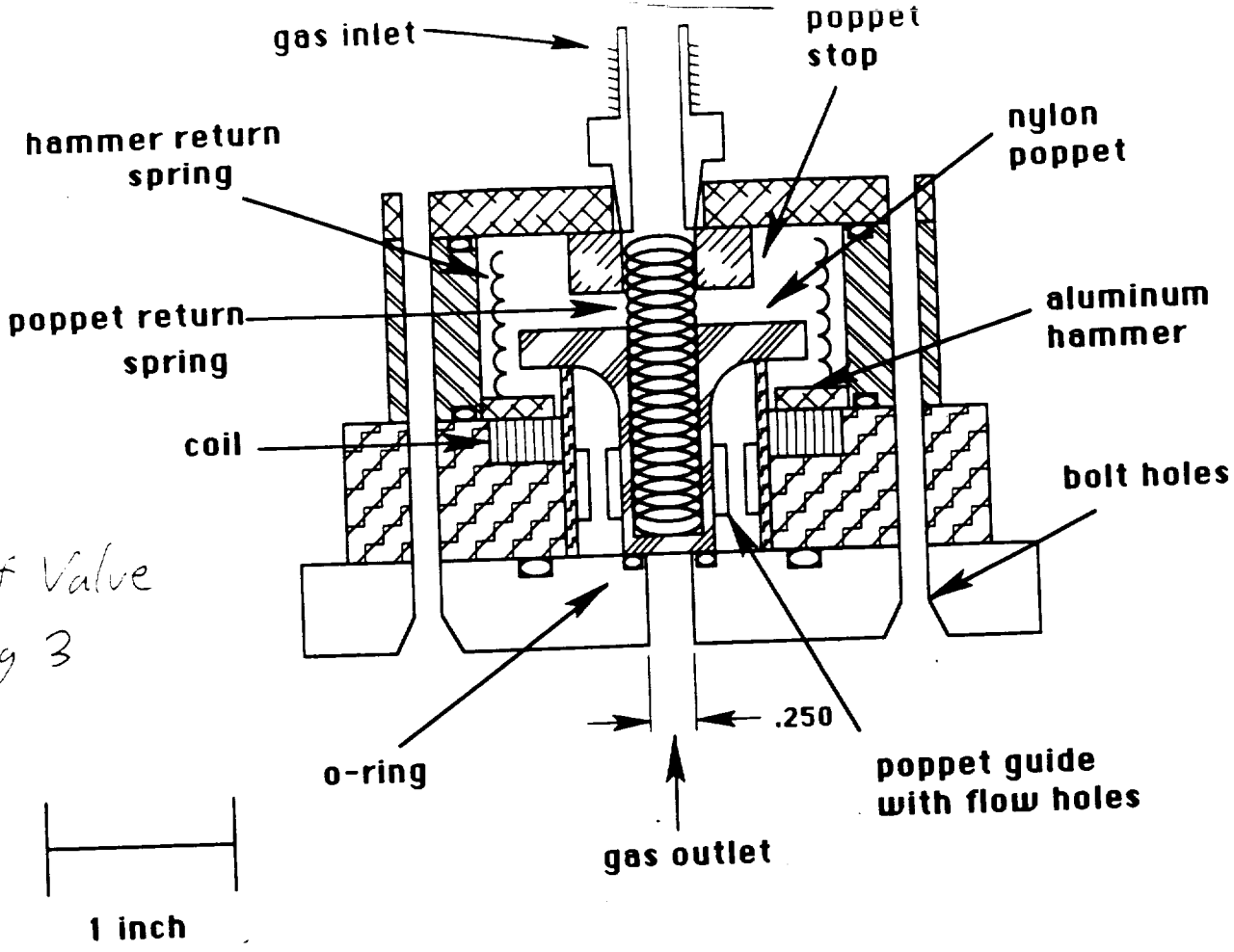

Puff Valve
Fig 3

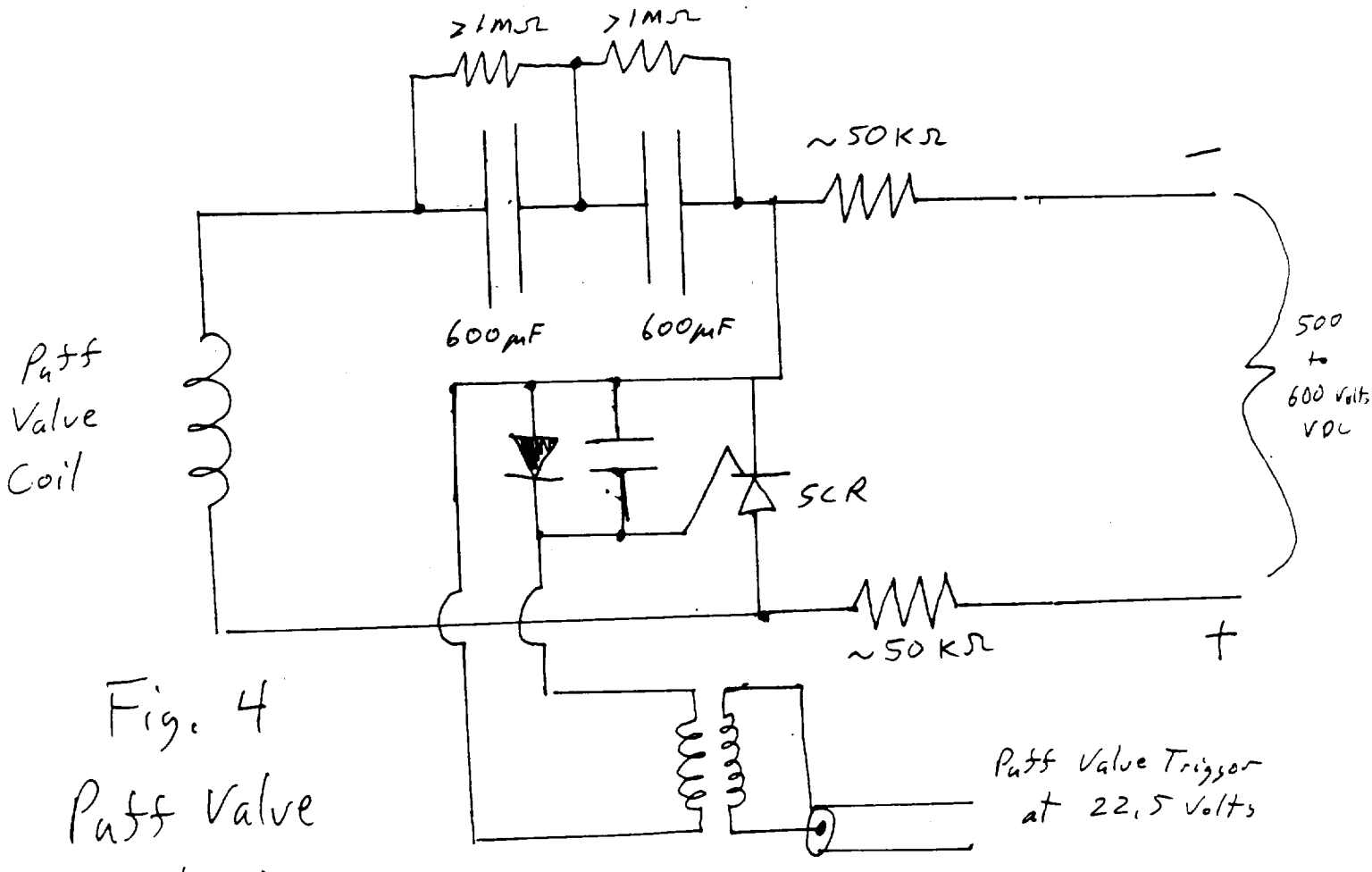

Fig. 4
Puff Valve
Electronics

Figure 4b (Rogowski Probe)

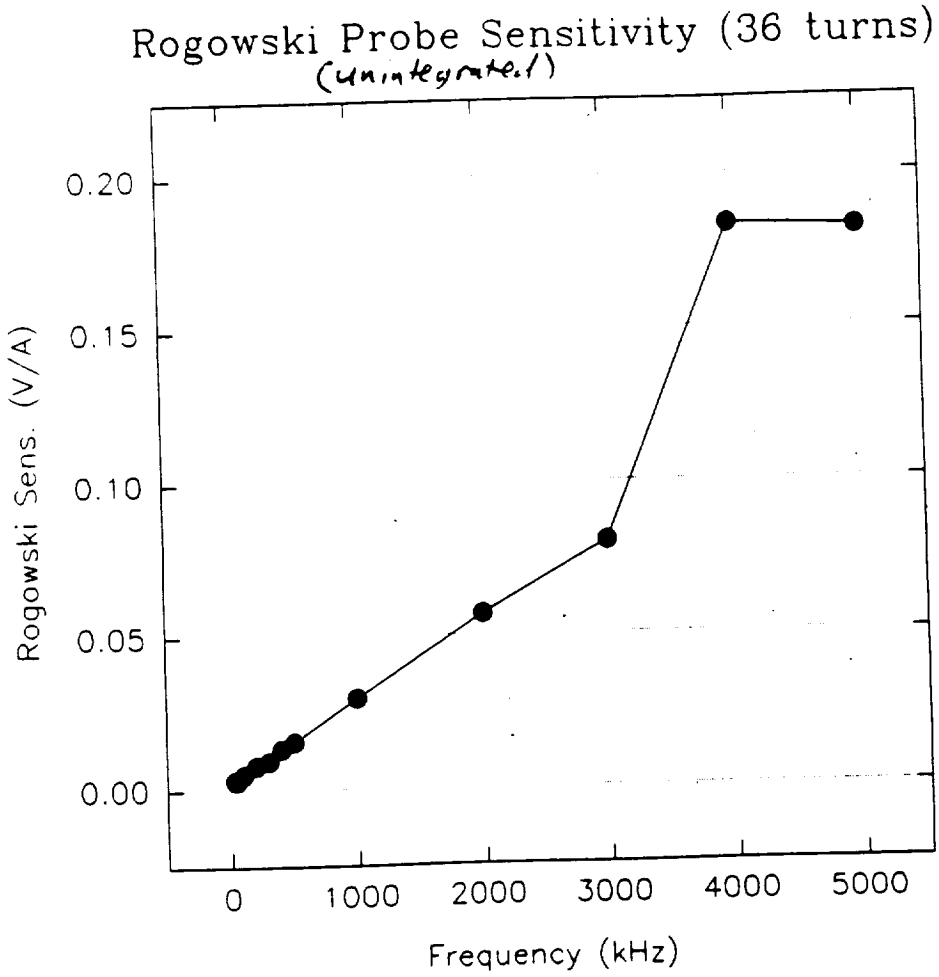

Rogowski Sensitivity

Freq. (kHz)	Pearson (mV)	Rog. (mV)	I (mA)	Sens. (V/A)
30	160	1	320	0.003125
40	160	1	320	0.003125
50	160	1	320	0.003125
100	150	1.5	300	0.005
200	160	2.5	320	0.0078125
300	160	3	320	0.009375
400	150	4	300	0.013333
500	160	5	320	0.015625
1000	160	9.5	320	0.029688
2000	150	17	300	0.056667
3000	150	24	300	0.08
4000	120	44	240	0.18333
5000	110	40	220	0.18182

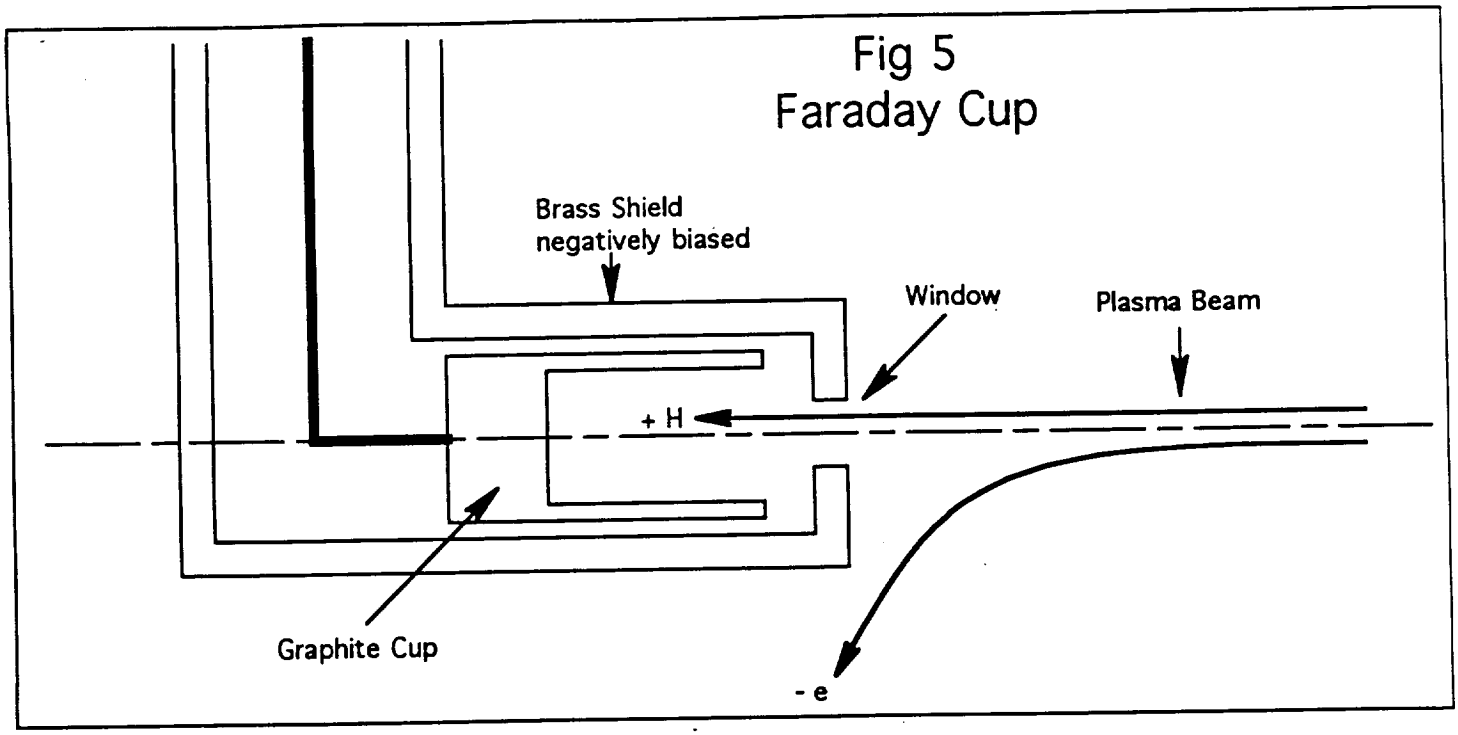
Fig 5
Faraday Cup
Brass Shield
negatively biased
Window
Plasma Beam
+ H
Graphite Cup
- e

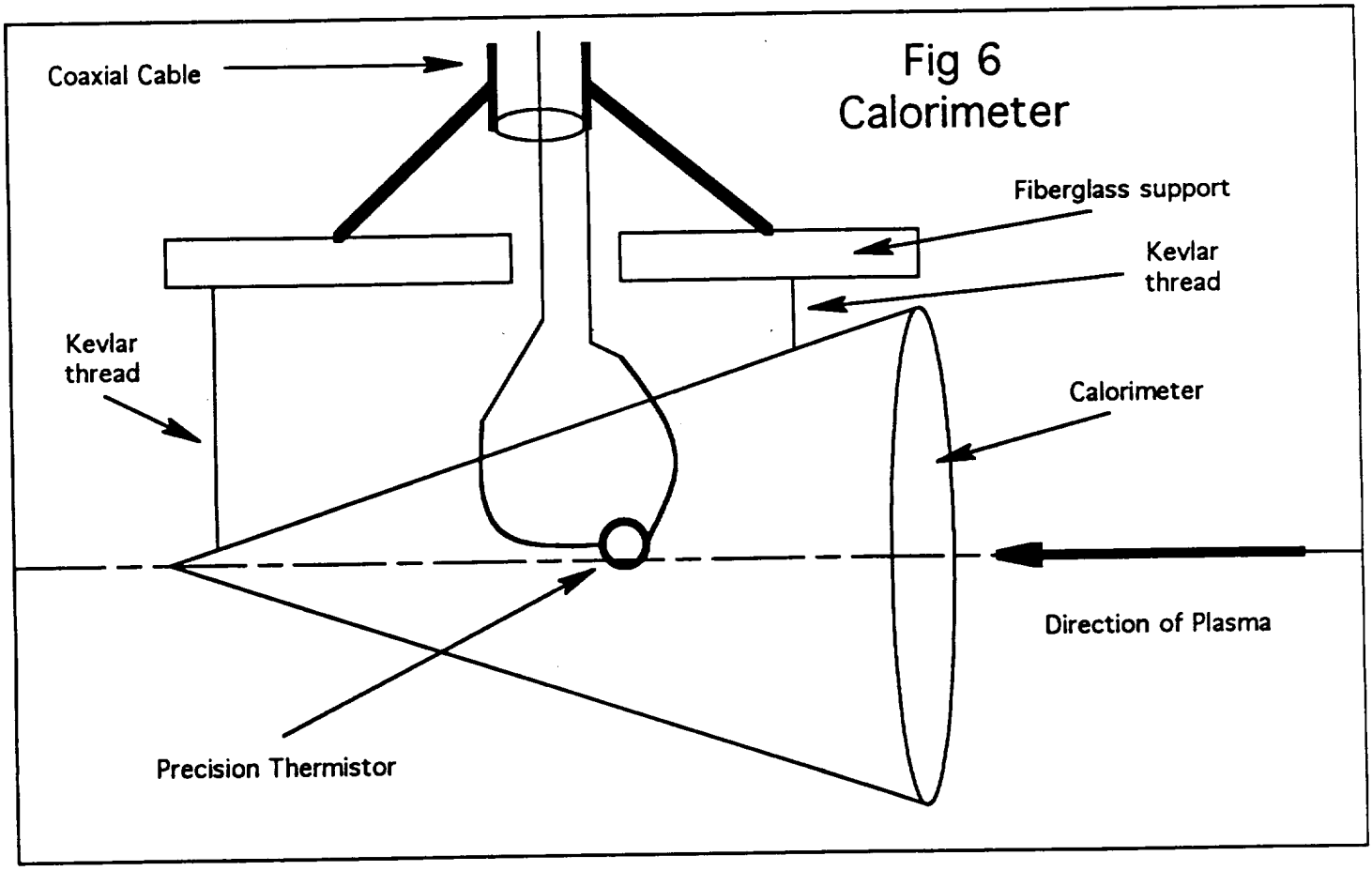
Fig 6
Calorimeter
Coaxial Cable
Fiberglass support
Kevlar
thread
Kevlar
thread
Calorimeter
Direction of Plasma
Precision Thermistor

Current

8/11/92

→ Made new strip line:

Brass shim stock ≈ 0.010" Thick
Printed Circuit board - etched
~~Used~~ Used rosen soder
roughly 30cm X 30cm

8/12/92

Test of New Stripline (with Brass Shim)

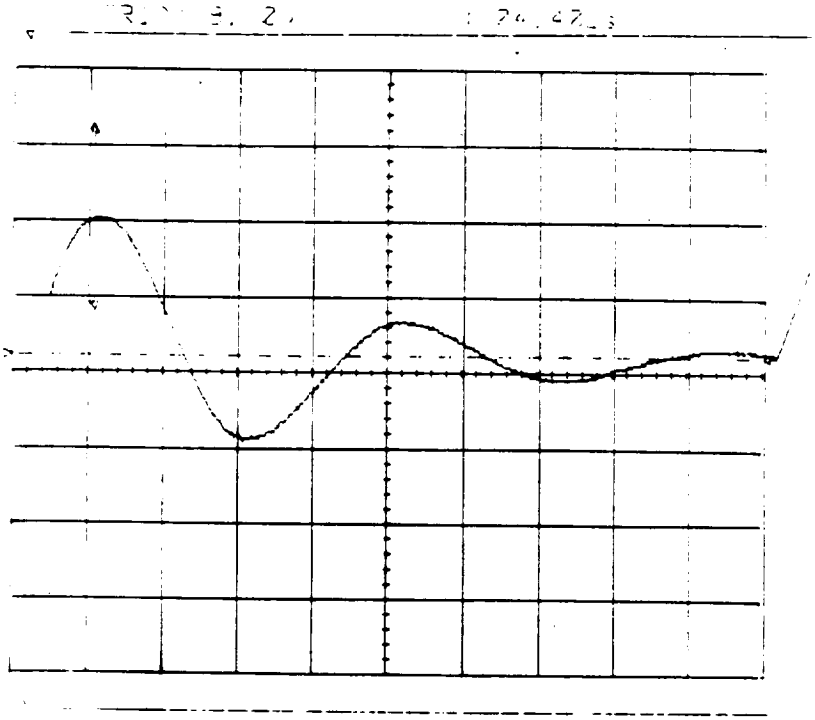

Rogowsky Integrated
≈ 23 kAmp/V

9.10 V * 23.164 kA/V ≈ 211 kA

Gun Voltage : 8.08 kV Gas type : Air

Pass Voltage : 506 V Pressure (tank) : 4.4×10^{-5} torr

Gas Pressure : 50 psi Current Rogowski : 211 kAmps

→ time to Max current = 4 μsecs

$\nu = T^{-1} = 22\,\mu sec^{-1} = 45.5$ kHz

Figure 8, Radial Profile

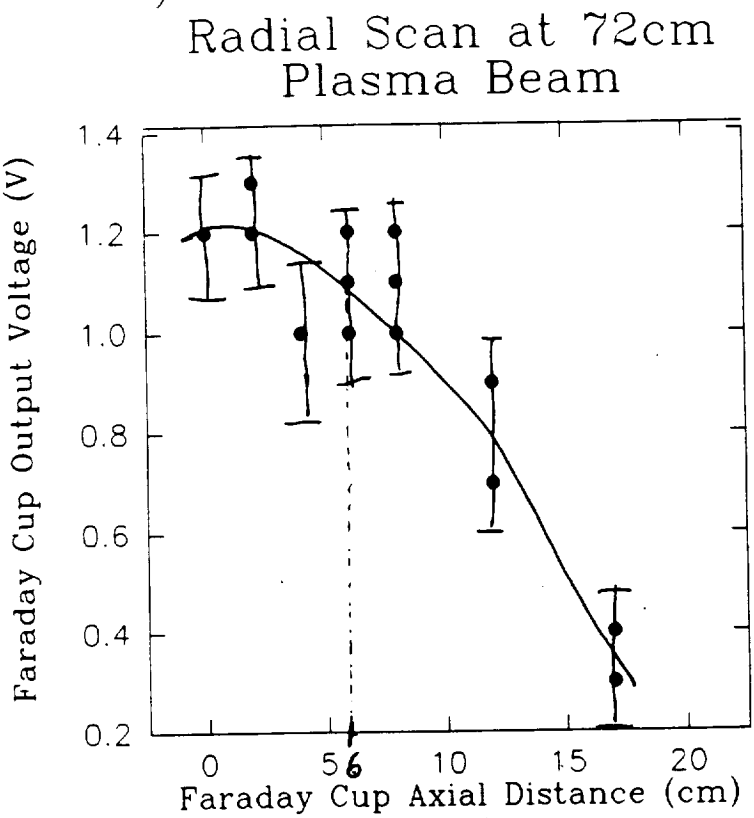

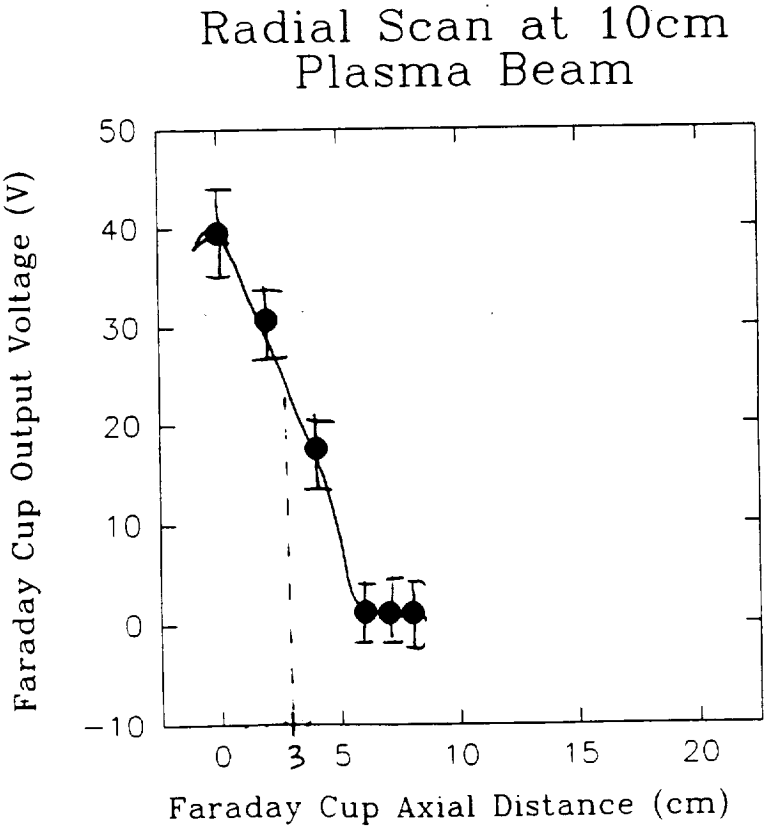

Figure 9 Radial Profile

RADSCAN.SPG: Wed, 19-Aug-92

F.C. Pos (cm)	FC Volt. (V)	F.C. Pos (cm)	FC Volt. (V)
0	1.2	0	39.6
0	1.2	2	30.8
0	1.2	4	17.6
2	1.3	6	1.1
2	1.2	7	1
2	1.2	8	1
4	1		
4	1		
4	1		
6	1		
6	1.2		
6	1.1		
8	1.2		
8	1.2		
8	1.2		
8	1		
8	1.1		
8	1.1		
12	0.9		
12	0.9		
12	0.9		
12	0.9		
12	0.7		
12	0.7		
17	0.4		
17	0.3		
17	0.3		

10 cm

72 cm

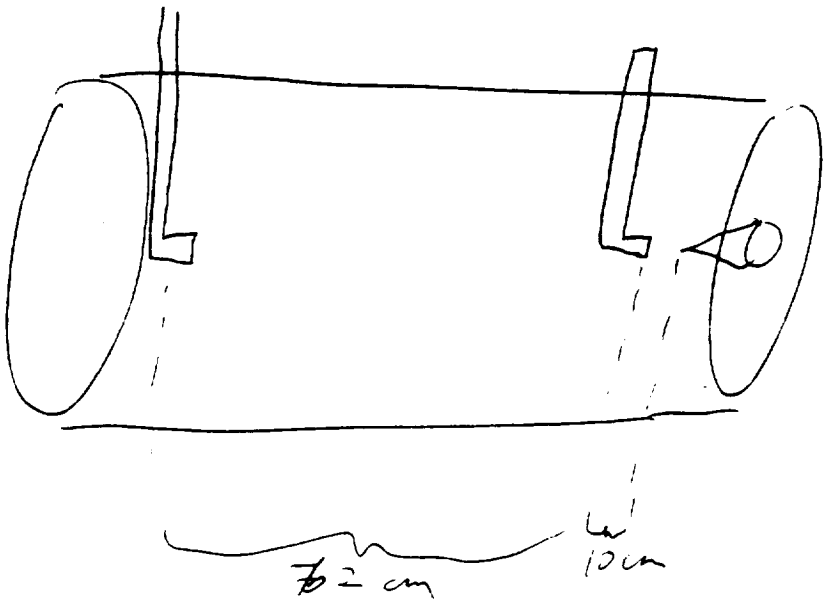

-8 kV, H_2, -100 V Fcup #8 ② off axis = 2 cm up 4x10⁻⁵ torr

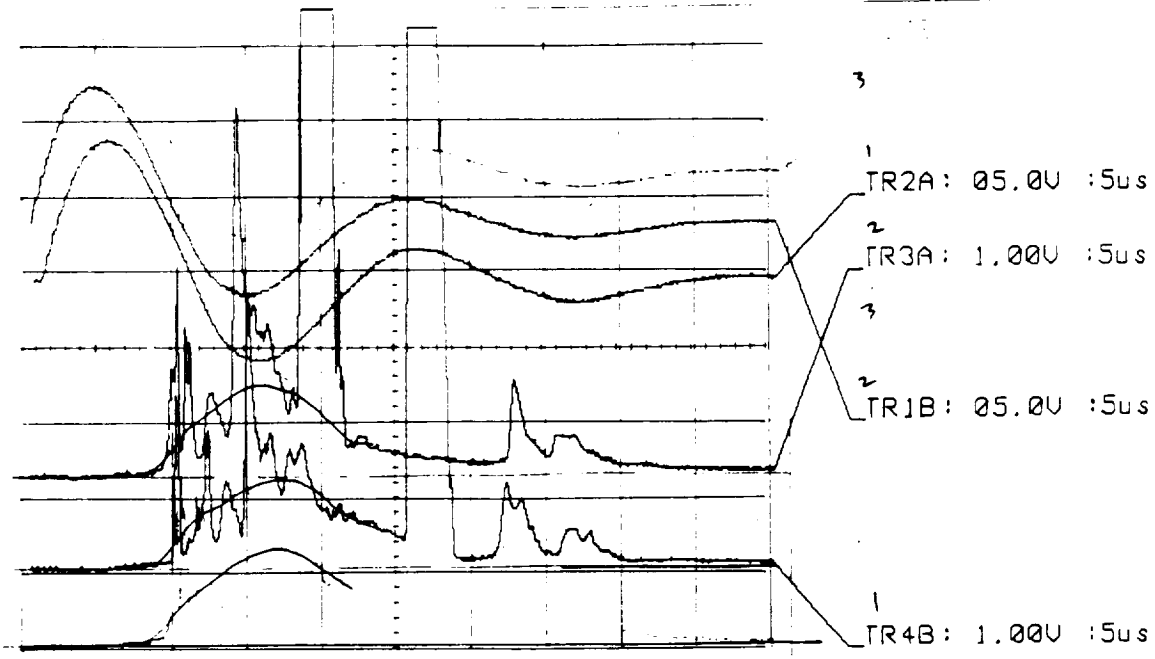

-8 kV, H_2, -100 V Fcup #8 ③ off axis = 4 cm up 4x10⁻⁵ torr

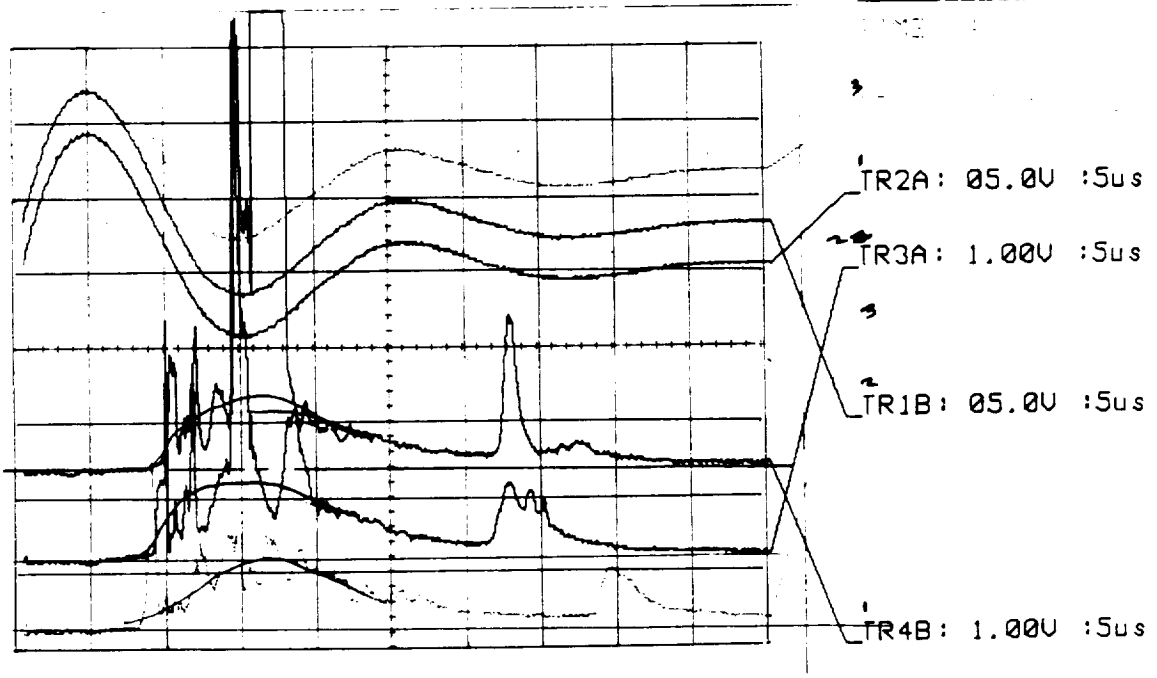

Test strip line V_G = 2kV, F.C. bias = 50V (P ~10 Torr)

Strip line works better than previous configuration:

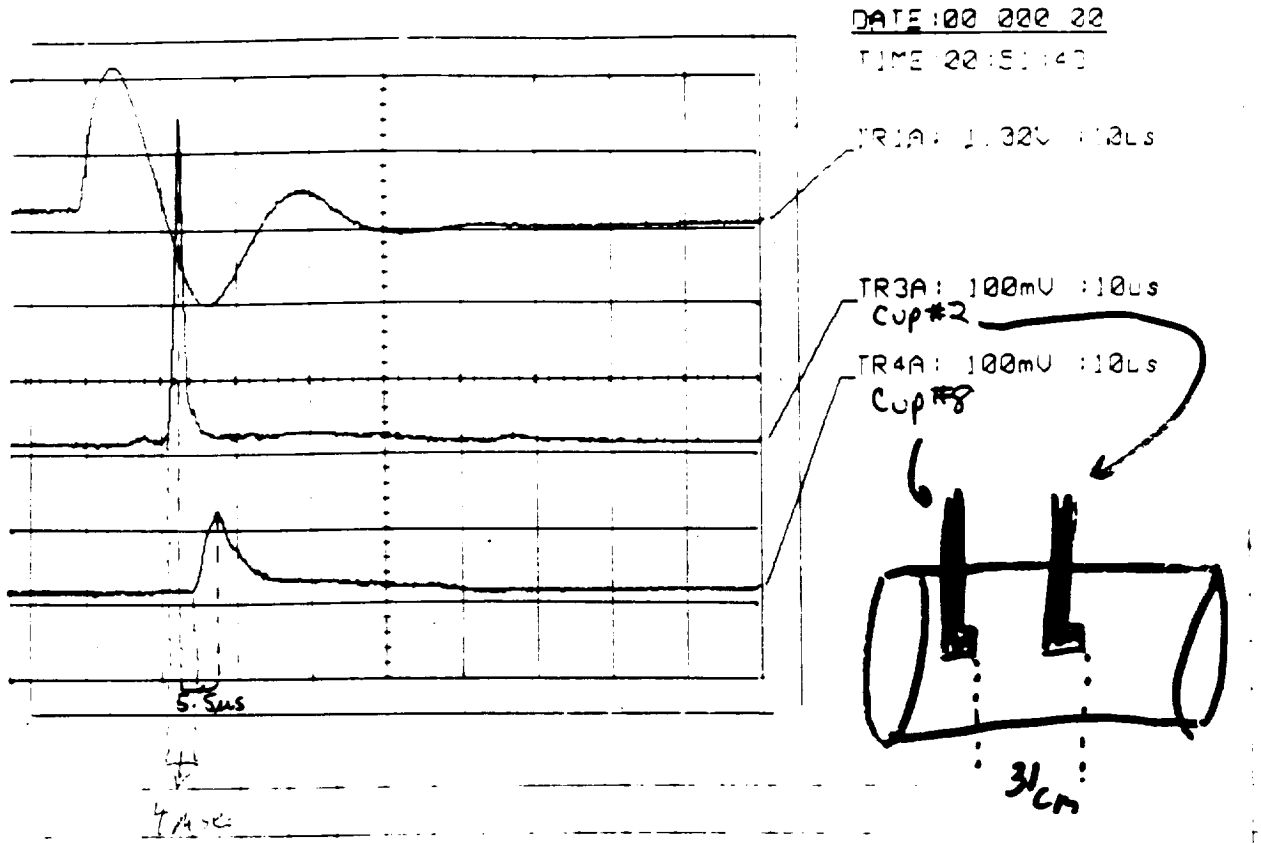

Velocity Calculation

8kV - H₂, Vcup ≈ 50V